Journal of Medicinal Chemistry

pubs.acs.org/jmc Article

Series of Novel and Highly Potent Cyclic Peptide PCSK9 Inhibitors Derived from an mRNA Display Screen and Optimized via Structure-Based Design

Candice Alleyne, Rupesh P. Amin, Bhavana Bhatt, Elisabetta Bianchi, J. Craig Blain, Nicolas Boyer, Danila Branca, Mark W. Embrey, Sookhee N. Ha, Kelli Jette, Douglas G. Johns, Angela D. Kerekes, Kenneth A. Koeplinger, Derek LaPlaca, Nianyu Li, Beth Murphy, Peter Orth, Alonso Ricardo, Scott Salowe, Kathleen Seyb, Aurash Shahripour, Joseph R. Stringer, Yili Sun, Rodger Tracy, Chengwei Wu, Yusheng Xiong, Hyewon Youm, Hratch J. Zokian, and Thomas J. Tucker*

Cite This: https://dx.doi.org/10.1021/acs.jmedchem.0c01084 Read Online

ACCESS | Metrics & More | Article Recommendations | Supporting Information

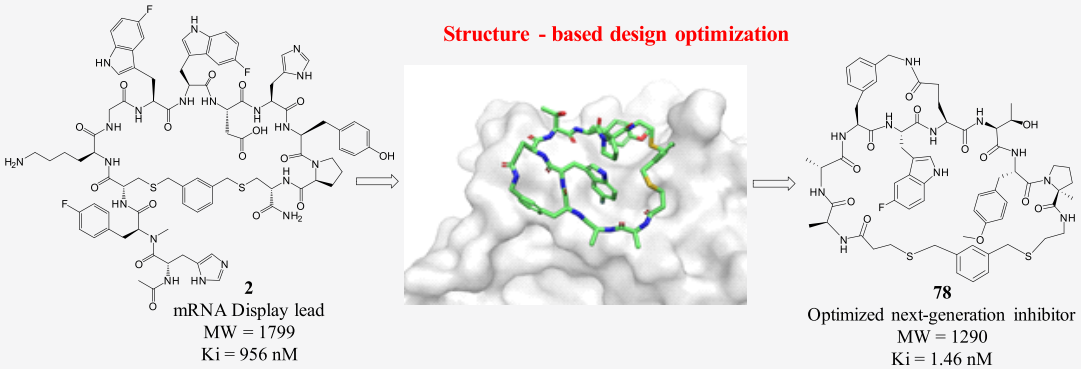

ABSTRACT: Proprotein convertase subtilisin-like/kexin type 9 (PCSK9) is a key regulator of plasma LDL-cholesterol (LDL-C) and a clinically validated target for the treatment of hypercholesterolemia and coronary artery disease. In this paper, we describe a series of novel cyclic peptides derived from an mRNA display screen which inhibit the protein−protein interaction between PCSK9 and LDLR. Using a structure-based drug design approach, we were able to modify our original screening lead **2** to optimize the potency and metabolic stability and minimize the molecular weight to provide novel bicyclic next-generation PCSK9 inhibitor peptides such as **78**. These next-generation peptides serve as a critical foundation for continued exploration of potential oral, once-a-day PCSK9 therapeutics for the treatment of cardiovascular disease.

INTRODUCTION

Proprotein convertase subtilisin-like/kexin type 9 (PCSK9) is a key regulator of plasma LDL-cholesterol (LDL-C) and an important target for treating coronary artery disease.[1] In genetic studies, it was demonstrated that humans heterozygous for specific gain-of-function truncation or missense PCSK9 mutations (∼2−3% of the population) have a 15−40% reduction in plasma LDL-C and a 50−90% reduction in the risk of CHD.[1] It has also been demonstrated via similar genetic data that humans who express specific loss-of-function mutations in PCSK9 have severe hypercholesterolemia and a high risk of coronary artery disease.[1]

The mechanism for the effect of PCSK9 on LDL-cholesterol (LDL-C) is well defined. PCSK9 in circulation decreases LDL-C levels by binding to the LDL-receptor (LDLR) on the cell surface, and the resulting endocytosis and lysosomal degradation serves as a key regulatory mechanism for LDL-C levels.[1] Direct blockade of the LDL-receptor−PCSK9 interaction therefore serves to increase the steady-state levels of LDLR, making more LDLR available to assist in the clearance of circulating LDL-C.[1] There are currently two commercial therapeutic antibodies (alirocumab[2] and evolocumab[3]) that have been approved for the treatment of familial hypercholesterolemia and for lowering LDL-C levels in patients who are not at goal via statin therapy. Phase III outcome studies with both have shown beneficial effects on cardiovascular events but demonstrated effects on lowering

Received: August 3, 2020

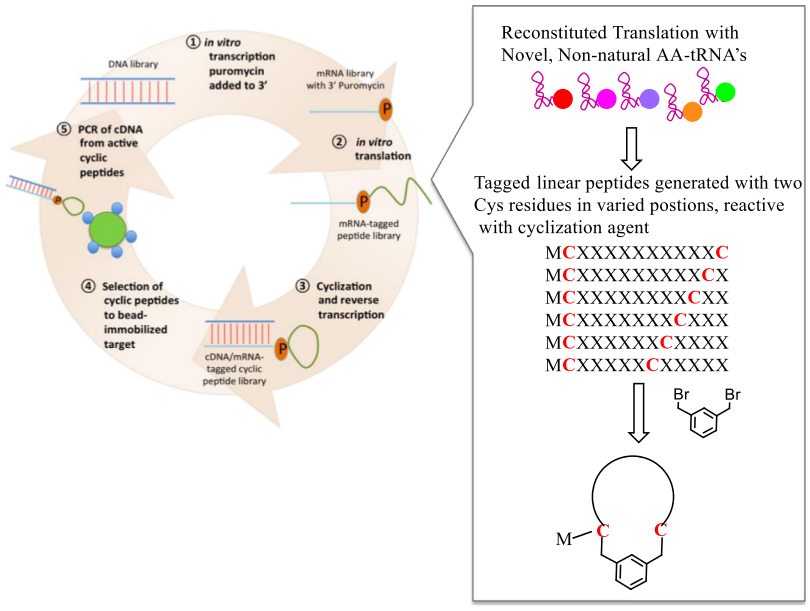

Figure 1. mRNA display approach using Ra Pharma Platform.

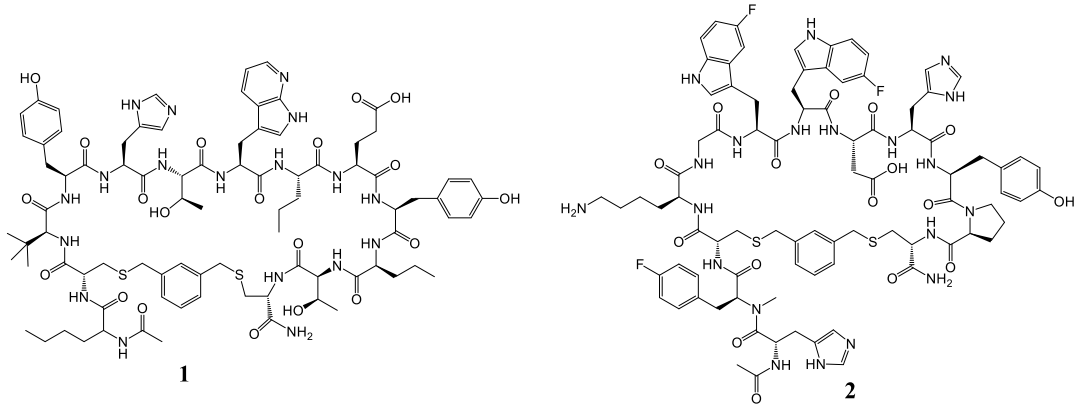

LDLR Fret Ki = 134 nM
MW = 1760
13 amino acids

LDLR Fret Ki = 956 nM
MW = 1890
12 amino acids

Figure 2. Two lead series derived from mRNA display screening.

overall mortality await further data.[2,3] These antibodies are administered subcutaneously either biweekly or monthly, and their initial uptake in the marketplace has not been as large as anticipated largely because of pricing pressures.[4]

It is estimated that of the approximately 70 million patients treated with statins, as many as 50% do not reach their target LDL-C levels.[5,6] Of those that do achieve treatment goals, another several million suffer major cardiovascular events annually.[5,6] The need exists for additional therapeutic options for those that do not achieve their LDL-C goals, patients with familial hypercholesterolemia, patients that do achieve goal but have cardiovascular events, patients with other comorbidities such as type 2-diabetes mellitus, and also in statin-intolerant patient populations. An oral, once daily PCSK9 inhibitor therapy could potentially offer a more convenient alternative for administration and better patient adherence. The orally delivered therapy of this type would easily align with other oral therapies that are standard of care in the at-risk population and would provide the benefit of easy dosing and level control compared to parenteral administration. Another benefit would be the ease of therapy withdrawal by simply discontinuing the dosing regimen.

Based on these factors, we chose to develop novel inhibitors of PCSK9 with the goal of eventually developing oral therapeutics for the treatment of hypercholesterolemia and coronary artery disease. Strategically, our intent was to develop PCSK9 inhibitors that generate equivalent LDL-C lowering to the established mAb standards evolocumab[2] and alirocumab.[3] The target of such inhibitors would be to orthosterically block the protein−protein interaction (PPI) between PCSK9 and LDLR by binding to the large, flat LDLR binding surface on the PCSK9 protein, thus preventing the direct interaction between the proteins.[1] The proteins and their interaction are well characterized in the literature,[7] and this provided a well-validated target for therapeutic intervention.[1] There are a large number of PCSK9 inhibitors reported in the literature, with several recent descriptions of novel small-molecule[8−11] and peptide[12−14] inhibitors, as well

https://dx.doi.org/10.1021/acs.jmedchem.0c01084
J. Med. Chem. XXXX, XXX, XXX−XXX

Scheme 1. General Approach to the Synthesis of Cyclic Peptides

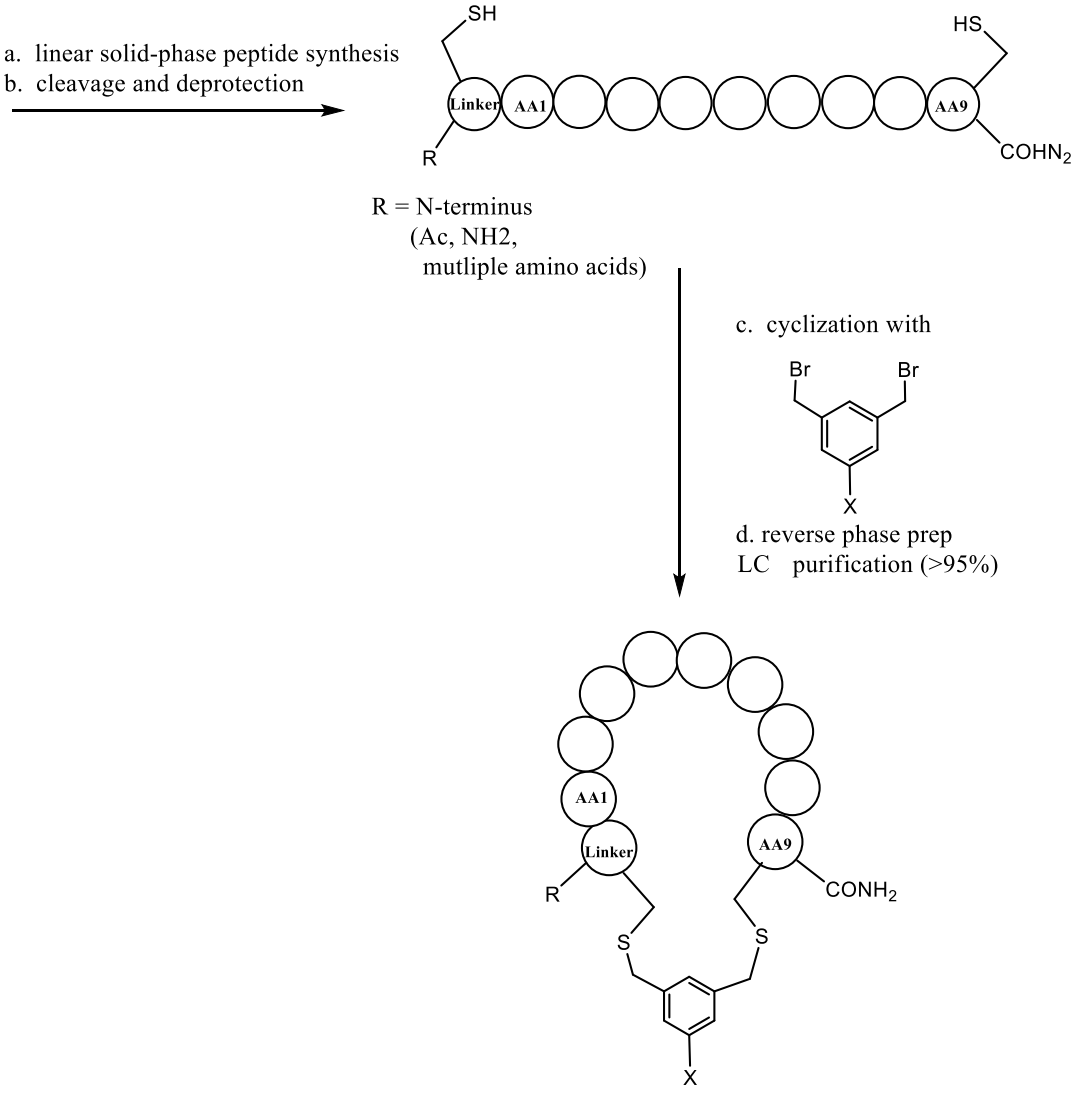

as siRNA-based therapeutics such as inclisiran.[15] The PCSK9 inhibitor area has recently been the subject of several comprehensive reviews.[16−18] However, none of the known inhibitors have the overall profile of potency and favorable druglike properties necessary to be viable as oral therapeutic agents.

We chose to initially pursue macrocyclic peptides as our modality of choice because of their potentially superior stability characteristics[19] as well as their proven ability to bind to the large, flat surfaces that are characteristic of PPIs such as the interaction between PCSK9 and LDLR. In collaboration with our partner Ra Pharmaceuticals,[20] we used the mRNA display technology to find potent, cyclic peptide inhibitors of PCSK9 that we could then engineer using internal medicinal chemistry expertise to be deliverable via oral dosing. The use of mRNA display as a proven and powerful platform for early hit finding is well documented in the literature.[20,21] Herein, we detail our initial screening hit peptides and the optimization of these macrocyclic peptides to provide highly potent, novel, and specific inhibitors of PCSK9 that serve as key starting points for the development of oral PCSK9 inhibitor therapeutics.

The initial mRNA display libraries of linear peptides of various lengths were prepared containing two reactive thiol moieties, allowing for direct cyclization of the libraries using the well-known 1,3-di(bromomethyl)benzene (DBX) as the key cross-linking element (Figure 1).[20] The DBX group is a commonly used and highly efficient cross-linking element for cyclization of peptide libraries derived from mRNA display.[20] From an initial series of mRNA screens targeting cyclic peptides of various sizes, we obtained two novel hit series (Figure 2). Compound **1** (Figure 2) was identified as a potent 13 amino acid hit with good potency against PCSK9 using the LDLR-FRET assay. A second, less potent but structurally unique 12 amino acid series was also found, with compound **2** (Figure 2) emerging as the key lead molecule from this series. The initial comparisons of the two series showed less overall homology, and analysis strongly suggested differing binding modes for each of the molecules. An early critical goal for the team was to obtain crystal structures of each of these representative structures bound to the LDLR binding site on PCSK9. We quickly obtained a crystal structure of the chemical series exemplified by **1** but were not able to initially obtain a structure for **2** or any early analogues, likely because of the large differences in potency between the two series, and

https://dx.doi.org/10.1021/acs.jmedchem.0c01084
J. Med. Chem. XXXX, XXX, XXX−XXX

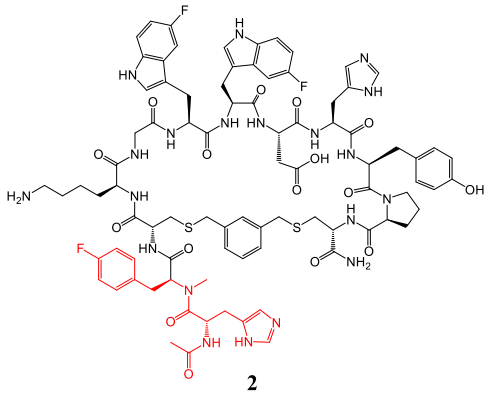

2

LDLR Fret Ki = 956 nM ± 0.7

remove two N-terminal "lasso" amino acids

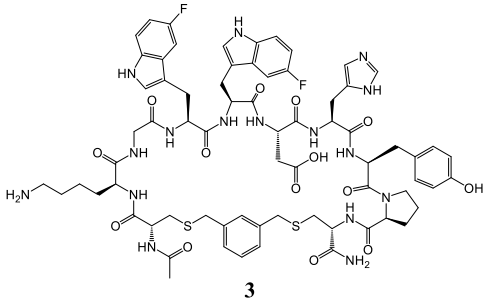

3

LDLR Fret Ki = 47.1 nM ± 1.5

completely remove N-terminus

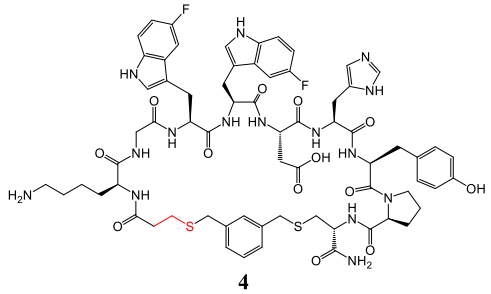

4

LDLR Fret Ki = 110 nM ± 1.3

Amino acid scans in Table 3

remove C-terminus

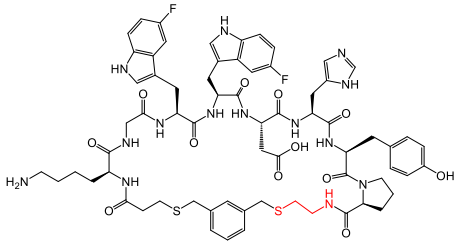

29

LDLR Fret Ki = 252 nM ± 21

add alpha -Me Pro

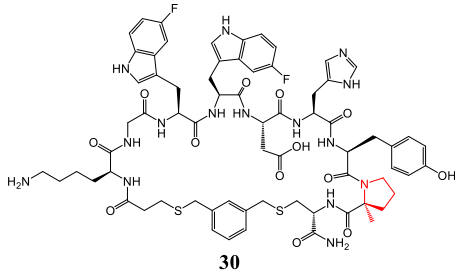

30

LDLR Fret Ki = 14.0 nM ± 1.6 (n =12)

Alexa-Fret Ki = 4.0 ± 1.0 nM (n = >200)

Figure 3. Early progression of SAR from original mRNA display lead **2**. Key structural changes are highlighted in red for clarity.

https://dx.doi.org/10.1021/acs.jmedchem.0c01084
J. Med. Chem. XXXX, XXX, XXX−XXX

Table 1. Mouse IV PK Parameters for Various Compounds[a,b,c,d,e]

compound number	AUC_{0-inf} (nM h)	AUC_{0-x} (nM h)	clearance (mL/min/kg)	V_{dss} (L/kg)	$T_{1/2}$ (h)	protein binding[d] (% bound, mouse plasma)
4[b]	241.93 ± 66.81	240.9 ± 42.20	51.73 ± 15.23	0.70 ± 0.48	1.04 ± 0.11	95.02
30[b]	181.43 ± 45.51	184.73 ± 45.34	65.40 ± 14.10	1.2 ± 0.59	0.33 ± 0.33	94.85
40[b]	491.78 ± 44.53	490.65 ± 43.34	24.25 ± 1.55	0.29 ± 0.13	0.78 ± 0.03	99.23
44[b]	2505.11 ± 164.56	2494.04 ± 157.65	4.62 ± 0.29	0.10 ± 0	0.25 ± 0.03	99.90
53[c]	171.52 ± 3.03	170.56 ± 3.35	17.25 ± 0.25	0.37 ± 0	1.60 ± 0.29	98.33
78	840.94 ± 174.30	839.90 ± 174.25	16.00 ± 3.30	0.23 ± 0.11	0.66 ± 0.09	98.50

[a]Compounds were tested in C57BL/6 mice at 1 mpk using a 30% propylene glycol/70% PBS vehicle at a concentration of 0.5 mg/mL or at 1 mpk using a 20% DMSO/60% propylene glycol/20% water vehicle at a concentration of 1 mg/mL. [b]For compounds **4**, **30**, **40**, and **44**, the values are the average of three mice from a single experiment with the standard deviations noted. [c]For compounds **53** and **78**, the values are the average of two mice from a single experiment, and the indicated errors are the difference between the mean and the individual values. [d]All protein binding values are derived from a single experiment. [e]Raw concentration vs time profiles for all compounds are provided in the Supporting Information, along with T_{max} and C_{max} data.

Table 2. Stability of Key Compounds against Gut Proteases and Whole Blood[a]

compound #	chymotrypsin, 1 h (% remaining)	elastase, 1 h (% remaining)	pepsin, 1 h (% remaining)	trypsin, 1 h (% remaining)	mouse whole blood $T_{1/2}$ (min)	Cyno whole blood $T_{1/2}$ (min)
4	12	60.7	95	1.2	63.2	ND
5	15.5	54.9	92.5	1.0	89.6	ND
30	10.9	52.7	94	0.9	311.3	>360
39	7.4	46.1	99.1	0.8	333.5	ND
40	42.7	99.1	93.7	79.5	186.1	>360
41	20.1	96.5	96.6	91.0	>360	>360
44	76.4	100	100	94.3	>360	ND
50	91	51	95	1.9	>360	ND
52	91	56	99.5	1.2	62	186
53	100	100	98.1	95.9	>360	ND
60	24.2	68.2	87.5	98.4	>360	ND
62	39.5	96.3	98.6	96.0	>360	ND
75	91.8	96.6	98.9	99.2	ND	>360
78	2.5	100	98.2	100	>360	113
79	95.7	98.8	94.4	97.6	>360	>360

[a]Compounds were incubated in duplicate in a single experiment for 1 h at 37 °C; ND indicates that the value was not determined for the specific molecule.

had to rely primarily on empirical data and molecular modeling based on that data. Details of the efforts around **1** will be described in another paper currently in preparation.[22] The current manuscript will focus on the optimization of the lead molecule **2**, initially using standard empirical medicinal chemistry strategies, which were later coupled with advanced structure-based drug design approaches.

RESULTS AND DISCUSSION

Screening and Early Structure–Activity Relationship. Test peptides were initially evaluated for PCSK9 inhibition activity using an LDLR-FRET assay (described in the Experimental Section), and the results are initially reported as IC_{50} values. In general, the peptides were synthesized using standard solid-phase peptide synthesis (SPPS) approaches to prepare the crude linear peptides after cleavage and deprotection (Scheme 1). The crude peptide could then be easily cyclized by addition of 1,3-di(bromomethyl)benzene (DBX), followed by purification to give the desired cyclic peptide products (Scheme 1). Specific synthetic details are provided in the Experimental Section. Starting from compound **2**, we envisioned an approach by which we would attempt to reduce the size and molecular weight of the target peptides while also simultaneously addressing the potency and peptide stability. Starting with the N-terminal lasso "tail" region, we were quickly able to remove the amino acids in the tail to provide **3** (Figure 3), which demonstrated a 20-fold improvement in potency in our LDLR-FRET assay. Further truncation of the N-terminus to completely remove it provided **4**, which lost only about 2-fold potency versus **3** (Figure 3). Compound **4** became a key early analogue for our program, and we decided to characterize overall properties in more depth. We wanted to address the stability of our cyclic peptide platform early on and chose to evaluate our peptides against a series of important gastrointestinal proteases (trypsin, chymotrypsin, pepsin, and elastase) for ultimate oral dosing and in whole blood for intravenous (IV) dosing. Early IV PK studies were primarily performed in C57BL/6 mice to keep the amount of compound needed from synthesis at a minimum. Table 1 summarizes the IV PK for a number of molecules discussed throughout this paper, and Table 2 details the observed protease and whole blood stability. Compound **4** was shown to have a short half-life and moderately high clearance in the mouse, and the whole blood stability indicated a moderate half-life in mouse whole blood of about 1 h. The protease panel clearly showed poor stability in the presence of chymotrypsin, elastase, and trypsin. For **4**, and in general across all the peptides tested, full stability to pepsin was observed. Metabolite identification (Met ID) studies after incubation with each of the key proteases also showed major

https://dx.doi.org/10.1021/acs.jmedchem.0c01084
J. Med. Chem. XXXX, XXX, XXX−XXX

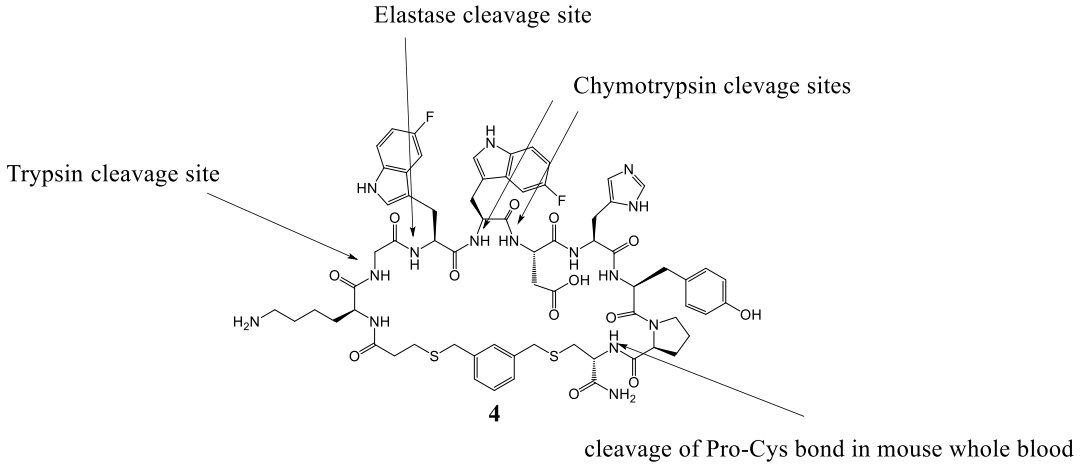

Figure 4. Primary metabolic sites on a representative molecule based on met ID studies with key proteases and mouse whole blood.

metabolic vulnerabilities at four amide bonds in the N-terminal region of the peptide (Figure 4), and we were able to correlate the most vulnerable individual amide bonds with the corresponding responsible protease. Met ID studies with the peptide after incubation in mouse whole blood showed a major metabolic site at the amide bond between the proline at position 8 and the cysteine at position 9 (Figure 4).

Alanine, D-alanine, and *N*-methyl amino acid scans were also performed using **4** as the scaffold. The results of these scans are summarized in Table 3. The alanine scan (Table 3, **5**−**12**) showed some tolerance for side chain modifications at positions 1 (Lys; **5**), 3 (5F-Trp at position 3; **7**), 5(Asp; **9**), and 6 (His; **10**). Interestingly, 5-fluoro-tryptophan (5F-Trp) at position 3 appeared to be much more amenable to change than the one at position 4. The D-amino acid scan (Table 3, **13**−**20**) showed less tolerance for D-amino acids, although position 2 (Gly) was not surveyed, and this would later become of importance. Similarly, the *N*-methyl amino acid scan (Table 3, **21**−**28**) showed less tolerance for backbone N-methylations, with the exceptions being positions 1 (Lys; **21**) and 7 (Tyr; **27**) where N-methylation appeared to be reasonably well tolerated.

Removal of the C-terminal amide of **4** provided **29** (Figure 3), which demonstrated a small 2-fold decrease in inhibitory potency but removed two H-bond donors. As indicated above, a metabolic liability was identified for the amide bond between proline and cysteine that we theorized was likely due to a prolyl-endopeptidase or similar enzyme, and we wanted to address this issue immediately. For this reason, the proline was replaced with an α-methyl proline to give **30**. Peptide **30** turned out to be a key molecule for the evolution of our entire program.

We observed an 8-fold improvement in inhibitory potency versus parent peptide **4** and much improved whole blood stability (Table 2), suggesting alleviation of the metabolic issue at this center. Despite having much improved stability in mouse whole blood, compound **30** (Table 1) was shown in the mouse to have a moderate clearance and extremely short half-life. The molecule demonstrated poor stability against our protease panel (Table 2).

In an attempt to explore some general structure−activity relationship (SAR) around the peptides, we initiated a broader survey of the SAR at several of the key positions along the peptide, using the peptide backbones from peptides **3** and **4**. Tables 4 and 5 summarize the key SAR around positions 3 and 4 (5F-Trp moieties) and 8 (proline), respectively. Of great interest were the unusual consecutive 5F-Trp moieties at positions 3 and 4. From the data in Table 4, it became quite clear that the 5F-Trp moiety at position 4 was playing a crucial role in the binding of the peptide. Replacement of 5F-Trp at position 3 with a simple tryptophan (Table 4, **31**) resulted in a small loss of potency. However, replacement of 5F-Trp at position 4 with a tryptophan (Table 4, **32**) resulted in a more pronounced 23-fold loss of potency. In addition, 5F-Trp at position 3 could be replaced with an alpha-naphthylalanine (Table 4, 1-Nal; **33**) with potency maintained. Replacement of 5F-Trp at position 3 with either a larger 4-phenylphenylalanine (Table 4; **34**) or a homophenylalanine (Table 4; **35**) demonstrated that while there was some tolerability at this position, larger or longer side chains were not well tolerated. Table 5 summarizes a few changes at the Pro moiety at position 8.

As stated earlier, the addition of an alpha-Me proline to the peptide provided an 8-fold potency enhancement versus **4** and was a key SAR element at this position. Opening the proline ring by replacement with a sarcosine provided **36**, which demonstrated a large potency loss. Replacement of the proline with a four-membered azetidine amino acid **37** provided only a slight loss of inhibitory potency versus **30**, while enlargement of the ring to a six-membered ring in **38** showed a substantial loss of inhibitory potency versus both **4** and **30**.

Crystal Structure of Compound 30. The most important aspect of the synthesis of compound **30** was that we were able to use this compound to generate the first cocrystal structure in this series with PCSK9. We were unable to generate suitable crystals with earlier inhibitors in this series, most likely because of the limited potency observed with these molecules. The crystal structure of **30** was incredibly informative in multiple dimensions and is shown in Figure 5. The peptide assumes an overall "doughnut-like", circular binding conformation, with the side chain of 5F-Trp at position 4 in the center of the doughnut, sticking into a small pocket on the relatively flat surface of the binding site. The fluorine sits nicely between the two H-bonded β-sheet regions of the protein, with the shallow pocket defined by the backbone NH and carbonyls of Gly 370, Val 380, Ser 381, and Ile 369 and the side chains of Ile 369, Ser 381, and Phe 379 (Figure 6). The structure suggests possible favorable direct

https://dx.doi.org/10.1021/acs.jmedchem.0c01084
J. Med. Chem. XXXX, XXX, XXX−XXX

Table 3. Alanine, D-Amino Acid, and *N*-Me Amino Acid Scans on 4[a]

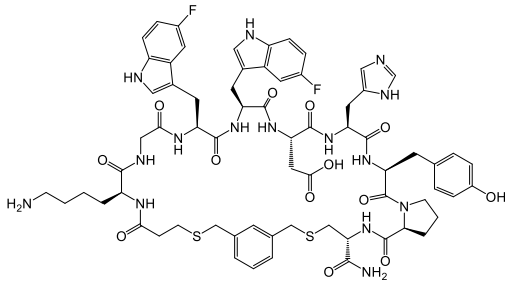

Compound	LDLR-FRET IC_{50} (n=2 ;nM)	Linker	AA Position 1	AA Position 2	AA Position 3	AA Position 4	AA Position 5	AA Position 6	AA Position 7	AA Position 8	AA Position 9
4	110±1.4	MPA	K	G	5F- Trp	5F- Trp	D	H	Y	P	Cys
5	392±104	MPA	**A**	G	5F- Trp	5F- Trp	D	H	Y	P	Cys
6	>48000	MPA	K	**A**	5F- Trp	5F- Trp	D	H	Y	P	Cys
7	656±100	MPA	K	G	**A**	5F- Trp	D	H	Y	P	Cys
8	>48000	MPA	K	G	5F- Trp	**A**	D	H	Y	P	Cys
9	427±115	MPA	K	G	5F- Trp	5F- Trp	**A**	H	Y	P	Cys
10	525±108	MPA	K	G	5F- Trp	5F- Trp	D	A	Y	P	Cys
11	>48000	MPA	K	G	5F- Trp	5F- Trp	D	H	**A**	P	Cys
12	>48000	MPA	K	G	5F- Trp	5F- Trp	D	H	Y	**A**	Cys
13	16232	MPA	**k**	G	5F- Trp	5F- Trp	D	H	Y	P	Cys
14	>48000	MPA	K	G	**w**	5F- Trp	D	H	Y	P	Cys
15	>48000	MPA	K	G	5F- Trp	**w**	D	H	Y	P	Cys
16	>48000	MPA	K	G	5F- Trp	5F- Trp	**d**	H	Y	P	Cys
17	>48000	MPA	K	G	5F- Trp	5F- Trp	D	**h**	Y	P	Cys
18	>48000	MPA	K	G	5F- Trp	5F- Trp	D	H	**y**	P	Cys
19	>50000	MPA	K	G	5F- Trp	5F- Trp	D	H	Y	**p**	Cys
20	2011	MPA	K	G	5F- Trp	5F- Trp	D	H	Y	P	**c**
21	342±120	MPA	**N-MeK**	G	5F- Trp	5F- Trp	D	H	Y	P	Cys
22	4090	MPA	K	**N-MeG**	5F- Trp	5F- Trp	D	H	Y	P	Cys
23a	>48000	MPA	K	G	**N-MeW**	5F- Trp	D	H	Y	P	Cys
23b	>48000	MPA	K	G	**N-MeW**	5F- Trp	D	H	Y	P	Cys
24a	>48000	MPA	K	G	5F- Trp	**N-MeW**	D	H	Y	P	Cys
24b	>48000	MPA	K	G	5F- Trp	**N-MeW**	D	H	Y	P	Cys
25	12867	MPA	K	G	5F- Trp	5F- Trp	**N-MeD**	H	Y	P	Cys
26	>48000	MPA	K	G	5F- Trp	5F- Trp	D	**N-MeH**	Y	P	Cys
27	112±20	MPA	K	G	5F- Trp	5F- Trp	D	H	**N-MeY**	P	Cys
28	>48000	MPA	K	G	5F- Trp	5F- Trp	D	H	Y	P	**N-MeCys**

[a]For all determinations, data is the average of $n = 2$, with the variability of the two determinations reported for molecules <1 μM. Data for the parent molecule **4** is highlighted in green. Purity of all peptides >95%; all peptides exhibited correct MS; MPA = 3-mercaptopropionic acid, all peptides cyclized from MPA to CYS using 1,3-di(bromomethyl)benzene (DBX). For peptides **14** and **15**, D-Trp was substituted for the unavailable D-5F-Trp; for peptides **23** and **24**, racemic *N*-Me Trp was used in the scans, and two diastereomers were recovered and tested for each; all were inactive.

interactions between the aryl fluorine atom and the NH of Gly 370, the carbonyl oxygens of Val 380 and Ile 369, as well as various interactions with the side chain carbons of the aforementioned amino acid side chains. Such noncovalent interactions between fluorine atoms and various amino acids are well documented in the literature.[23] The specific nature of the fit of the fluorine into this small surface pocket along with the previously described analogue work at this position confirms the critical nature of the interaction of the aryl fluoride with the small pocket on the PCSK9 surface. The selection of the 5F-Trp amino acid as one of the amino acids for the original mRNA display campaign was clearly critical to the entire screening and hit finding process with these peptides.

The lysine side chain at the N-terminal position 1 is fully solvent-exposed and does not appear to be making any specific interactions with the protein (Figure 5). The first 5F-Trp in the sequence at position 3 lies outside of the macrocyclic ring, opposite the inner 5F-Trp at position 4, partially solvent-exposed and contacting a lipophilic region consisting of the disulfide bond between Cys 375 and 378 and the side chains of Val 380 and Asp 374. The Asp−His region provides a turn-like geometry, with the Asp and His side chains of the inhibitor forming an ion pair that helps to lock this conformation. A key aspect of this entire N-terminal

https://dx.doi.org/10.1021/acs.jmedchem.0c01084
J. Med. Chem. XXXX, XXX, XXX−XXX

Table 4. SAR for Peptide Amino Acid Positions 3 and 4[a,b]

N-terminus -Lys-Gly-X-Y-Asp-His-Tyr-Pro-Cys-amide

compound #	N-terminus	X	Y	LDLR-FRET K_i (nM)
3	AcNHCys	5F-Trp	5F-Trp	47.2 ± 1.6
4	MPA	5F-Trp	5F-Trp	111 ± 1.3
31	AcNHCys	Trp	5F-Trp	103 ± 1.6
32	AcNHCys	5F-Trp	Trp	1070 ± 220[b]
33	MPA	1-Nal	5F-Trp	63 ± 1.7
34	MPA	4Ph-Phe	5F-Trp	29,345 (n = 2)[b]
35	MPA	homePhe	5F-Trp	2211 (n = 2)[b]

[a]FRET K_i values are the average of at least three determinations with the standard deviation indicated unless otherwise noted; MPA = 3-mercaptopropionic acid; alpha Nal = alpha-naphthylalanine; and 4-PhPhe = 4-phenyl-phenylalanine. [b]For n = 2, the error is reported for molecules <1 μM; error is defined as the difference between the mean and the individual determinations.

Table 5. SAR for Peptide Amino Acid Position 8 (Proline)[a]

MPA -Lys-Gly-(5F-Trp)-(5F-Trp)-Asp-His-Tyr-X-Cys-amide

compound #	X	LDLR-FRET K_i (nM)
4	Pro	115 ± 1.4
30	alpha-Me Pro	14.0 ± 1.7 (n = >200)
36	Sar	10,740 ± 20.3
37	Aze	67.5 ± 33.5
38	Pip	969 ± 110

[a]LDLR-FRET K_i values are the average of three determinations with the standard deviation noted unless otherwise indicated, except for **30**, which was used as an assay standard; Sar = sarcosine; Aze = 2(S)-azetidinecarboxylic acid; and Pip = 2(S)-piperidinecarboxylic acid.

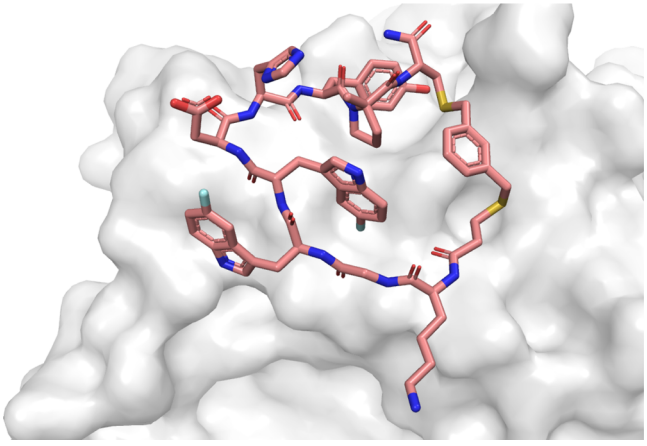

Figure 5. X-ray crystal structure of 30 (salmon) bound to the LDLR-binding site of PCSK9 at 1.55 Angstrom resolution (PDB: 6XIB). The molecule binds in an overall circular conformation, with 5F-Trp at position 2 outside of the doughnut and 5F-Trp at position 3 inside the macrocycle, with the fluorine atom in a small pocket on the surface. The side chains of position 1 (Lys), 5 (Asp), and 6 (His) are all solvent-exposed and do not directly interact with the protein. The side chain of position 7 (Tyr) lies in a small groove on the surface, and the aryl ring of the cross-linker lies directly on top of Ile 369.

region is the presence of five key hydrogen bonding interactions with a β-sheet on the protein that lies directly under the N-terminal region of the inhibitor. Figure 7 schematically details each of these H-bonding interactions, which can be characterized as follows:

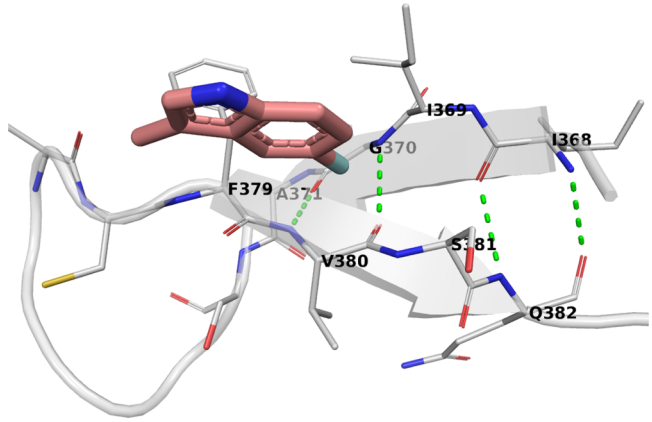

Figure 6. Close-up of the shallow binding pocket occupied by 5F-Trp in position 4 of **30**. The pocket is defined by two hydrogen-bonded beta sheets, with the aryl ring and 5-fluoro substituent of the ligand fitting downward into the space between.

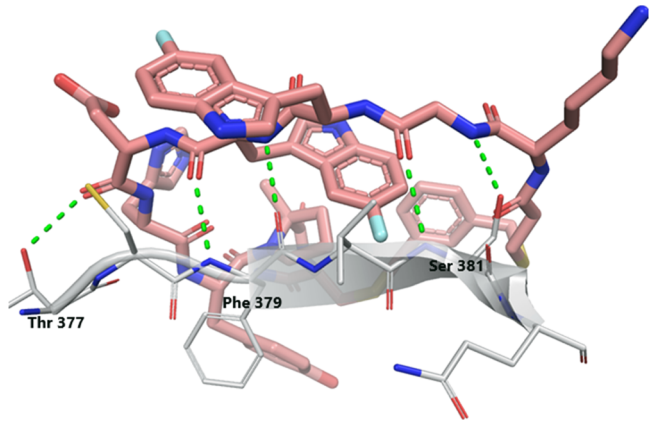

Figure 7. Schematic representation of the five key hydrogen bonding interactions between inhibitor **30** (salmon) and the PCSK9 active site β-sheet (white). The key interactions are described in detail in the text.

1. The NH of the glycine moiety in position 2 of the inhibitor makes an interaction with the side chain OH of Ser 381.
2. The carbonyl of the same glycine on the inhibitor makes an interaction with the backbone NH of Ser381.
3. The NH of 5F-Trp at position 3 of the inhibitor makes an interaction with the backbone carbonyl of Phe379.
4. The carbonyl of 5F-Trp at position 4 of the inhibitor makes an interaction with the backbone NH of Phe379.
5. The backbone carbonyl of the aspartic acid residue at position 5 of the inhibitor makes an interaction with the side chain OH of Thr377.

These key H-bonding interactions are critical for the good potency observed with these peptides. The tyrosine moiety of the inhibitor lies in one of the few true pockets in the binding surface (Figure 5). This shallow pocket is defined by the side chains of Phe379, Glu195, Asp238, and Ala239 and has a small, solvent-exposed opening near where the para-position of the tyrosine of the inhibitor resides. Interestingly, the proline ring sits quite close to the 5F-Trp side chain of the inhibitor that lies inside the macrocycle, suggesting a conformationally reinforcing intramolecular interaction between the two groups, likely reinforced further by the addition

https://dx.doi.org/10.1021/acs.jmedchem.0c01084
J. Med. Chem. XXXX, XXX, XXX−XXX

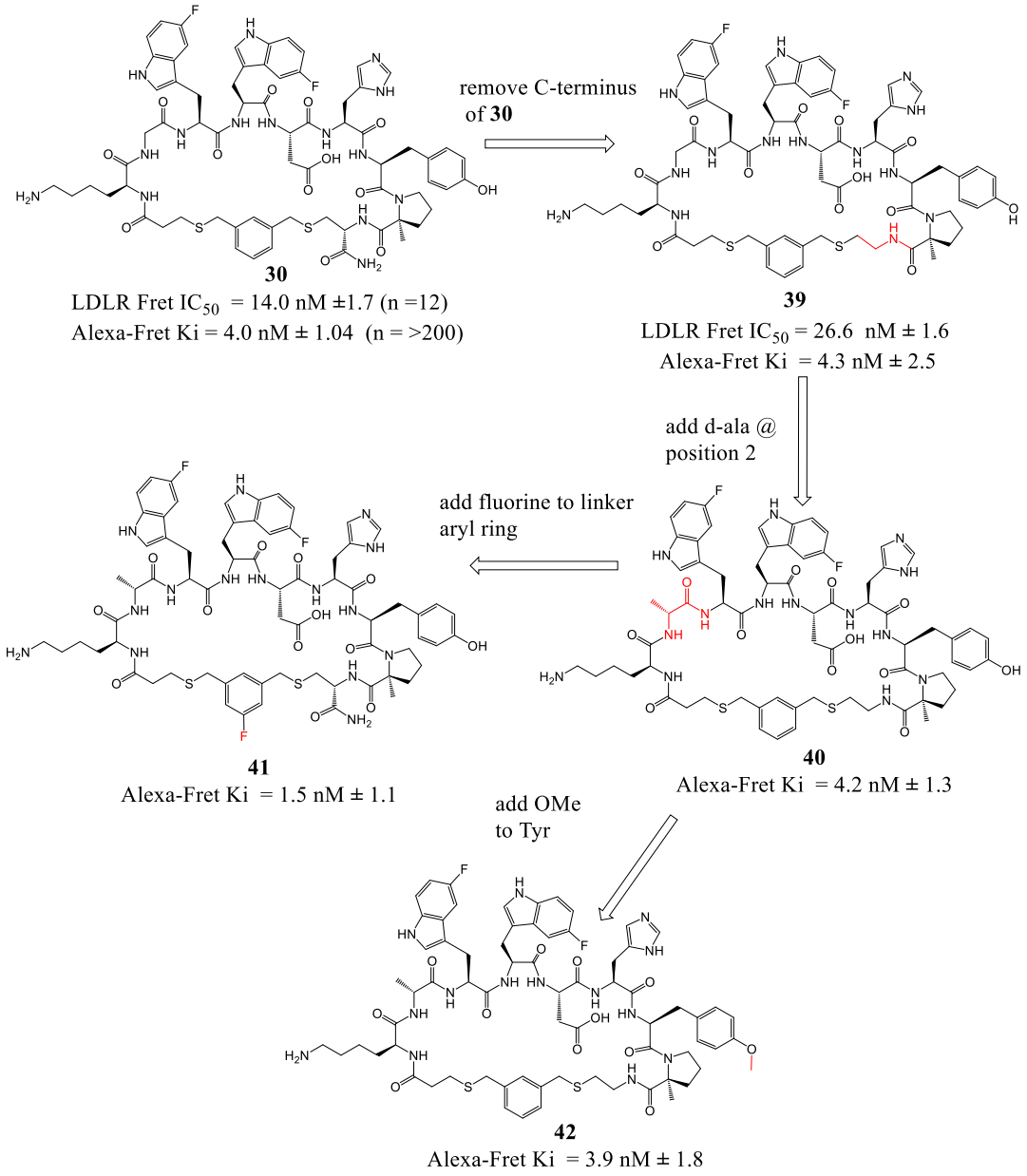

Figure 8. Continued SAR evolution of key lead molecules.

of the potency enhancing alpha-methyl group to the proline. These intramolecular interactions appear to be crucial for locking the molecule into a desirable conformation for binding. The C-terminal amide is largely solvent-exposed and does not interact with the protein, suggesting that it is likely not critical for binding, as suggested by data from compound **29**. Finally, to our surprise, we observed that the DBX cross-linking group was contributing to potency and directly interacting with the PCSK9 surface. The aryl ring lies directly above the side chain of Ile 369, almost sitting directly on top of the side chain in a manner analogous to a tabletop.

Expanded SAR around Compound 30. As we moved forward with analogues of improved potency, we began to observe a bottoming of the LDLR-FRET values and differentiation between compounds below the 10 nM range became difficult. We therefore established a second, more accurate Alexa-FRET assay that was able to better distinguish between compounds with more potent inhibitory potency (Experimental Section). The values for both assays are reported for a number of compounds to allow for comparison, but we eventually moved completely to the Alexa-FRET assay for more optimized molecules.

In addition to the key binding insights described above, the crystal structure of **30** also provided several critical design insights that would prove to be the key to driving subsequent efforts (Figure 8). We removed the C-terminus of **30** to provide **39**, which demonstrated minimal loss of potency and a similar behavior in our stability assays (Table 2). The β-sheet binding region also contains the four protease-labile amide bonds previously identified in these molecules (Figure 4). Although the alanine scan with **4** (Table 3) clearly indicated that an alanine was not tolerated at position 2 (Gly) because of a likely unfavorable interaction with 5F-Trp that lies inside the macrocycle, the crystal structure of **30** strongly suggested that a D-alanine would be well tolerated at this position. The region that would be occupied by a substituent

https://dx.doi.org/10.1021/acs.jmedchem.0c01084
J. Med. Chem. XXXX, XXX, XXX−XXX

of a D-amino acid points away from the protein and into an open, solvent-exposed region in parallel with the side chain of Lys at position 1. We theorized that using a D-amino acid at this position might also help to block some of the metabolism observed in this region of the molecule. We therefore prepared the analogue **40** containing a D-alanine at position 2 (Figure 8). This molecule was shown to be essentially equipotent with **30** and **39**. **40** was shown to have improved stability versus both elastase and trypsin, the enzymes responsible for proteolysis at the two amide bonds flanking the D-alanine at position 2 (Table 2). Therefore, our strategy to insert a D-amino acid at this position based on the crystallographic data from **30** appeared to be successful, allowing for the stabilization of two of the four vulnerable amide bonds. Interestingly, the mouse whole blood stability of **40** decreased slightly but was still quite good. However, **40** still showed a short half-life after IV dosing to mice (Table 1). Nonetheless, the noted improvement in protease stability became a key feature for future compound design. Figure 9 shows the crystal structure of **40**; it is superimposable with the previously shown structure of **30**, with the addition of the key D-alanine moiety at position 2. The methyl group of the D-amino acid can be clearly seen pointing away from the protein and pointing toward solvent. It is also easy to see why an L-amino acid side chain is not tolerated at this position as indicated in the alanine scan, as it would likely bump the indole ring system of the key 5F-Trp moiety at position 4, causing a displacement of this critical interaction.

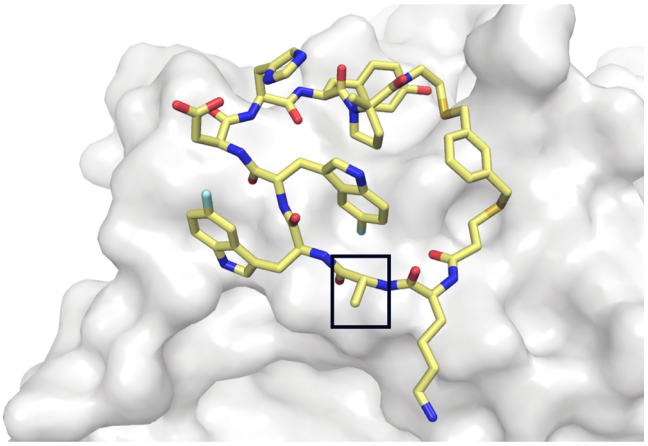

Figure 9. X-ray crystal structure of 40 (lt. yellow) bound to the LDLR binding site on the surface of PCSK9 at 1.38 Angstrom resolution (PDB: 6XIC). The molecule binds in an identical manner as **30**, with the methyl group of the D-Ala at position two (highlighted in the black box) pointing away from the protein toward the solvent. The D-amino acid at this position also blocks proteolytic degradation at the two flanking amide bonds caused by trypsin and elastase activity.

Based on the crystal structure of **30**, it was observed that there was some space available on the aryl ring of the DBX cross-linker to put a substituent in the position meta to the two sulfurs. Adding a fluorine to this position provided **41** (Figure 8), which added a small amount of potency versus **40** but did not add any additional stability to the peptides (Table 2), with the peptide remaining vulnerable to chymotrypsin proteolysis at the remaining two previously identified amide bonds. In addition, we also capped the OH of the tyrosine aryl ring at position 7 with a methyl group to give **42**, which retained similar potency to **40** but eliminated an H-bond donating group, an SAR item that could be of interest for later designs targeted at optimizing permeability/oral bioavailability.

To more broadly understand the scope and limitations of the D-amino acid side chain at position 2, we also prepared several direct analogues of **40** with various D-amino acids replacing the D-alanine. The results of this small SAR scan are detailed in Table 6. Lipophilic side chains such as those on **43**, **44**, **47**, and **48** were all well tolerated, as were polar side chains such as **45** and **46**. In addition, **46** demonstrates that while the stereochemistry of the two centers is different, the substitution on positions 1 and 2 is likely interchangeable because both of these side chains point away from the protein and into solvent. The SAR in general suggested that position 2 was extremely tolerant and could likely be exploited via a wide variety of substituents and might later be useful as a handle for modifying solubility and physical properties or for adding various labels. In addition, **44** was screened for IV PK in the mouse; however, it displayed a similar short half-life to earlier analogues (Table 1). Compound **44** also showed a protease stability profile similar to **40** (Table 2), although the bulkier side chain of **44** did appear to be able to impact the vulnerability to chymotrypsin as well.

Discovery of Pro−Thr Backbones to Replace Asp−His. At this point, we wanted to take advantage of the finding that the D-amino acid could add stability and wanted to couple this with other changes in the backbone to address the other metabolically labile amide bonds. In examining the

Table 6. SAR for D-Amino Acids at Position 2[a]

MPA -X-Y-(5F-Trp)-(5F-Trp)-Asp-His-Tyr-Pro-cysteamine

Compound #	X	Y	LDLR-Fret Ki (nM)	Alexa -Fret Ki (nM)
40	Lys	D-Ala	23.3 ± 1.1	4.2 ± 1.3
43	Lys	D-Nvl	43.5 ± 1.2	2.7 ± 0.6
44	Lys	D-Val	17.6 ± 1.4	6.3 ± 1.2
45	Lys	D-Thr	26.9 ±1.2 (n = 2)	ND
46	Ala	D-Lys	48.1 ± 4.4	ND
47	Lys	D-Cpg	ND	23.1 ±1.2 (n =2)
48	Lys	D-Tbg	ND	4.2 ± 2.8 (n =3)

[a]All values are the average of at least three determinations unless otherwise indicated; standard deviation is indicated for all $n > 2$; for $n = 2$, the reported error is the difference between the mean and the individual; values. D-Nvl = D-norvaline; D-Val = D-valine; D-Thr = D-threonine; D-Lys = D-lysine; D-Cpg = D-cyclopentyl gly; and D-Tbg = D-*tert*-butyl glycine. ND = not determined.

https://dx.doi.org/10.1021/acs.jmedchem.0c01084
J. Med. Chem. XXXX, XXX, XXX−XXX

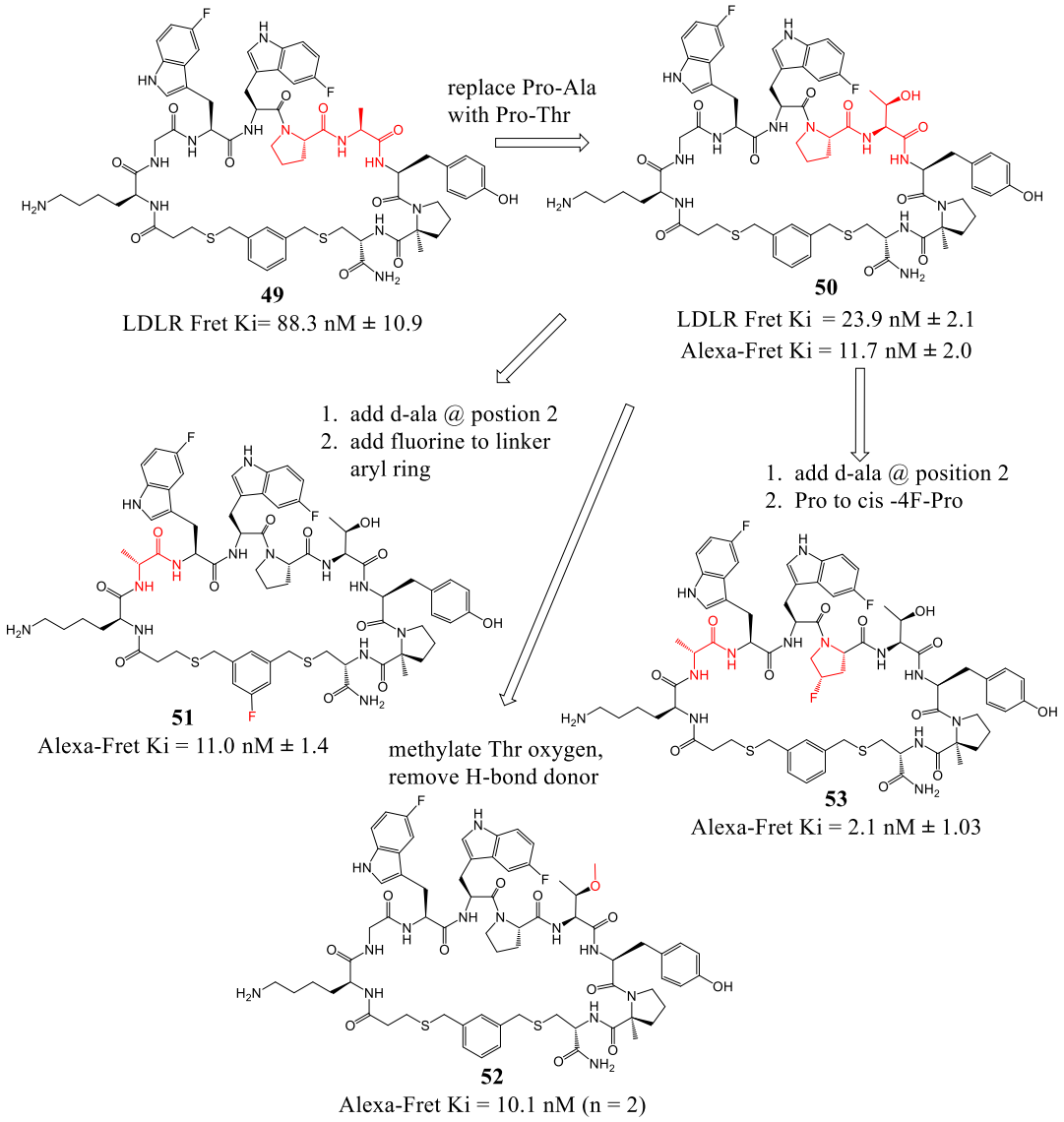

Figure 10. Pro-Ala and Pro-Thr as replacements for Asp-His at positions 5 and 6 of the macrocyclic peptide.

crystal structures of compounds **30** and **40**, it was apparent that the Asp−His amino acids at positions 5 and 6 could be replaced with amino acids that could similarly mimic the turn-like geometry of this region. One simple replacement that immediately came to mind was Pro−Ala. The Pro−Ala dipeptide could serve as a simplified mimetic of Asp−His, while also using the five-membered ring of the proline to mask an additional NH, which we hoped would in turn stabilize one of the remaining two metabolically labile amide bonds. Figure 10 details the progression of several analogues based on Asp−His replacements. The simple Pro−Ala analogue **49** showed the viability of this modification, although some inhibitory potency was lost. The Pro−Thr analogue **50** regained some of the lost potency. Combining this Pro−Thr backbone change with the D-alanine at position 2 and the meta fluoro-DBX linker (previously shown in **41**) provided analogue **51**. We were able to obtain a crystal structure of compound **51** (Figure 11), which showed that Pro−Thr was a super-imposable replacement for Asp−His with similar levels of potency and the ability to mask an additional amide bond and hopefully stabilize this region further against chymotrypsin. The proline ring perfectly mimics the turn-like geometry of Asp−His, and the side chain of Thr does not interact directly with the protein and is solvent-exposed. The fluorine atom on the aryl ring is shown to occupy open space in the center of the macrocycle and may participate in and enhance the intramolecular interactions between the α-Me Pro and the indole ring of 5F-Trp at position 4. This intramolecular interaction may in turn help to further stabilize the overall conformation of the molecule.

Methylation of threonine OH to remove another H-bond donor provided **52**, which was equipotent with the unmethylated analogue. This change was performed to eliminate one H-bond donor from the molecule, and the addition or subtraction of a methyl group here did not appear to affect the potency or stability of the molecule greatly and as such were used interchangeably. Guided by the crystal structure, we were able to replace the proline in position 5 with the commercially available 4(*S*)-*cis* fluoroproline in an attempt to further increase the chymotrypsin stability. Combining this with the D-alanine at position 2 provided **53**, which showed a 4-fold increase in inhibitory potency.

https://dx.doi.org/10.1021/acs.jmedchem.0c01084
J. Med. Chem. XXXX, XXX, XXX−XXX

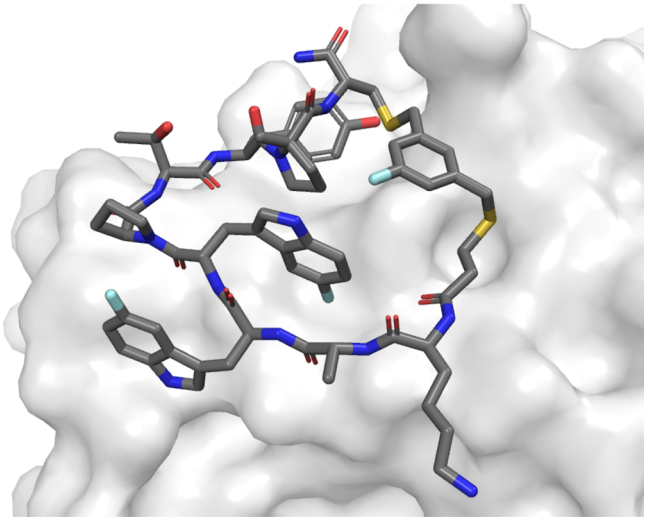

Figure 11. Crystal structure of 51 (gray) bound to the LDLR-binding site on PCSK9 at 1.48 Angstrom resolution (PDB: 6XID). The macrocyclic peptide binds similarly to the previously shown crystal structures, with the Pro-Thr providing an excellent replacement for the original Asp-His at positions 5 and 6. The Thr side chain hydroxyl is solvent-exposed and does not make any direct contact with the protein. The fluorine atom on the aryl ring is shown to occupy open space in the center of the macrocycle and may participate in and enhance the intramolecular interactions between the alpha-Me Pro and the inner 5F-Trp aromatic.

Compound **53** demonstrated very good stability against the entire panel of proteases including chymotrypsin and good stability in mouse plasma (Table 2). However, after IV dosing to mice, the compound was shown to have a moderate clearance and a relatively short half-life (Table 1). The introduction of a proline to this region appeared to help stability against some proteases; however, it did not solve the short *in vivo* half-life seen with these analogues despite their apparent improved *in vitro* stability. We therefore chose to pause work on Pro−Thr analogues.

Discovery and Remediation of Mast Cell Degranulation Activity. At this point, based on the observations from previous internal drug discovery programs, we became concerned about the potential for mast cell degranulation related to these peptides. We noted that all the molecules we were synthesizing contained a highly basic lysine side chain in an overall somewhat lipophilic framework. We had in previous peptide and peptidomimetic drug discovery programs correlated this generic structural phenotype in some cases with histamine release *in vivo*, likely because of the extensive mast cell degranulation activity.[24,25] In an effort to confirm this hypothesis, we tested several molecules in our rat mast cell degranulation assay (Table 7). For the three molecules initially screened, the results were striking. Moderately potent mast cell degranulation activity was observed for **4**, **30**, and **53**, all of which contained a lysine side chain in position 1 of the peptides.

However, we needed to gather additional data to support or disprove the mast cell degranulation hypothesis. We prepared a series of analogues at the position 2 lysine to try to directly confirm our initial hypothesis and also looked back at a few earlier analogues that were made at this position as well. Table 8 details the potency and rat mast cell degranulation activity for these Lys analogues (**54**−**66**). All these analogues

Table 7. Rat Mast Cell Degranulation Activity for Select Molecules[a]

compound #	position 1 amino acid side chain	rat mast cell degranulation (EC_{50}, μM)
4	Lys	positive@6.67
30	Lys	positive@6.67
53	Lys	positive@3.12

[a]Histamine release activity was determined in rat peritoneal mast cells, data for all compounds is the average of at least two determinations. Rat peritoneal lavage contains about 5% mast cells, which is sufficient to initiate a robust response (confirmed by the positive control 48/80); assay end point is histamine release in supernatant. Cells were incubated with test articles for 30 min in 1−3% DMSO. For all tested molecules and DMSO controls, there was no loss in cell viability up to 60 μM.

exhibited moderate to good inhibitory potency, again confirming the solvent-exposed nature of this substituent and the good tolerability to various changes at this position. A strong correlation was found between the basicity of the position 1 side chain and the observed mast cell degranulation activity. More basic, free amine side chain-containing amino acids such as ornithine (**55**) and epsilon *N*,*N*-dimethyl Lys (**61**) demonstrated mast cell degranulation activity, while the acidic side chain amino acids (**54**, **58**, **59**) and neutral side chain amino acids (**56**, **57**) were all negative in the assay. Interestingly, the permanently positively charged epsilon trimethyl Lys analogue **60** was also clean in our mast cell degranulation assay. Despite the potential stability issues and metabolic vulnerabilities based on the structure, **60** appeared to have superior solubility characteristics and we decided to evaluate the IV PK properties of the molecule. Peptide **60** was dosed IV to mice and demonstrated improved pharmacokinetics (PKs) with a relatively moderate clearance and 1.2 h half-life (Table 9).

Based on this result, **60** was also dosed IV in Wistar Han rats, again demonstrating much improved IV PK with a low clearance, 2.5 h half-life, and improved *in vivo* tolerability. This molecule demonstrated the best overall IV PK in rodents of any of the early molecules tested in this series. Acylating the lysine epsilon amino group with a peg as in **62** (synthesized as shown in Scheme 2) also eliminated mast cell degranulation activity, as did the addition of moderately basic side chain amines such as those in the PEGylated analogues **63** (synthesized as detailed in Scheme 2) and **66** (synthesized as detailed in Scheme 3). The SAR at this position clearly confirmed that free basic amino acid side chains such as Lys and Orn were major contributors to the observed mast cell degranulation activity and removing the basic amine or substantially moderating the basicity remediated the undesired activity. In general, the observed mast cell degranulation/associated histamine release appears to be a compound/series issue, directly related to the overall properties of the rest of the molecule that contains the offending basic group.[24,25] In general, most amine-containing drug-like molecules do not exhibit this activity; however, we have observed this phenomenon internally with a number of diverse molecules across various programs, suggesting that this behavior should be suspected anytime a molecule containing a basic amine side chain in a somewhat overall lipophilic framework demonstrates an unusual or idiosyncratic toxicity *in vivo*. Having obtained a reasonable understanding of this issue and

https://dx.doi.org/10.1021/acs.jmedchem.0c01084
J. Med. Chem. XXXX, XXX, XXX−XXX

Table 8. Lysine Analogues at Position 2: Inhibitory Potency and Rat Mast Cell Degranulation Activity for 70−63, 66[a]

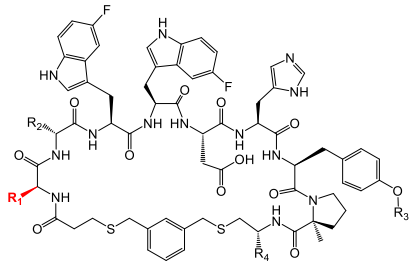

Compound #	Lys analog R1	R2	R3	R4	LDLR-Fret Ki (nM)	Alexa-Fret Ki (nM)	Rat Mast Cell Degranulation EC_{50} (μM)
control 48/80[b]							Positive @ 1 uM
54	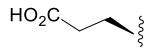	CH_3	H	H	202.2 ± 13.1	ND	negative
55	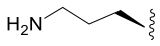	H	H	$CONH_2$	132.5 ± 2.4	14.3 ± 1.9	Positive @ 7 μM
56	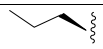	H	H	CONH2	94.7 ± 1.5	35.2 ± 9.2	negative
57	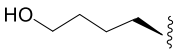	CH_3	CH_3	H	78.9 ± 2.6	39.0 ± 5.4	negative
58	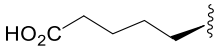	CH_3	CH_3	H	ND	85.8 ± 4.8	negative
59	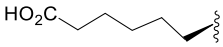	CH_3	CH_3	H	ND	80.7 ± 5.7	negative
60	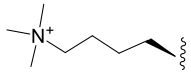	CH_3	CH_3	H	ND	9.5 ± 2.6	negative
61	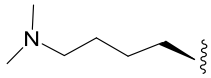	CH_3	CH_3	H	ND	4.2 ± 1.7	Positive @ 10 μM
62	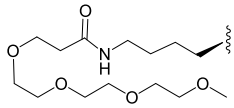	H	H	$CONH_2$	ND	9.4 ± 1.9	negative
63	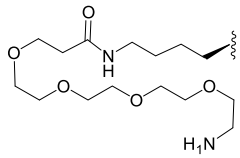	H	H	$CONH_2$	ND	10.7 ± 0.4	negative
66	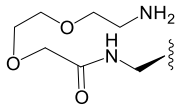	CH_3	CH_3	H	ND	8.2 ± 1.3	negative

[a]LDLR-FRET and Alexa-FRET data is the average of at least three determinations unless noted otherwise in table with standard error indicated; for $n = 2$, the difference between the mean and the individual data points is noted as the error. The histamine release activity was determined in rat peritoneal mast cells, data for all compounds is derived from at least two agreeing determinations. Rat peritoneal lavage contains about 5% mast cells, which is sufficient to initiate a robust response; assay end point is histamine release in supernatant. Cells are incubated with test articles for 30 min in 1−3% DMSO. For all tested molecules and DMSO controls, there was no loss in cell viability up to 60 μM. [b]48/80 (refs 24 and 33) is used as a positive control for the assay.

how to remediate it, we returned to our efforts to optimize the overall properties of our molecules.

Novel Cyclizations. Upon further studying the crystal structures of **30** and **51**, we were struck by several potential opportunities for novel cyclizations. From the crystal structure of **51**, it was apparent that there was more room in the space occupied by the fluorine atom on the DBX linker. In fact, the fluorine atom points directly at the NH of the indole of the inner 5F-Trp, suggesting that the two groups could possibly be linked together (Figure 12). We also chose to remove the

https://dx.doi.org/10.1021/acs.jmedchem.0c01084
J. Med. Chem. XXXX, XXX, XXX−XXX

Table 9. Mouse and Rat IV Pharmacokinetics for 60[a,b]

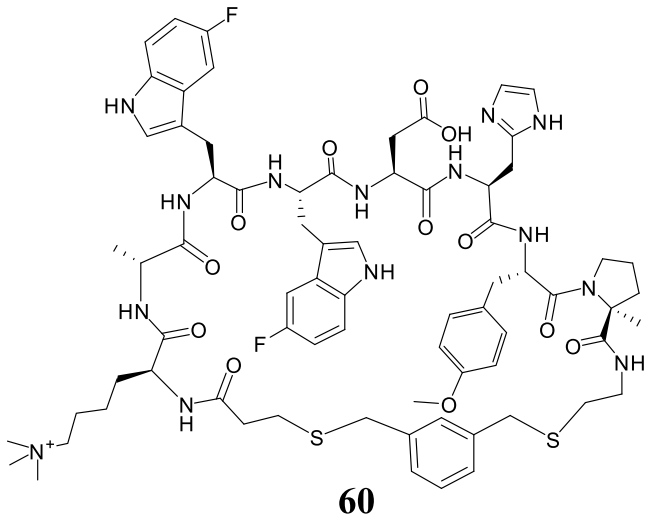

60

species	AUC_{0-inf} (nM h)	AUC_{0-x} (nM h)	clearance (mL/min/kg)	V_{dss} (L/kg)	$T_{1/2}$ (h)	protein binding[c] (% bound)
C57BL/6 mice[a]	932.72 ± 102.63	895.96 ± 70.06	6.20 ± 0.68	0.45 ± 0.07	1.16 ± 0.02	99.3
Wistar Han rat[b]	3648.33 ± 422.20	3646.9 ± 421.60	3.16 ± 0.40	0.17 ± 0.00	2.46 ± 1.34	99.9

[a]Compound was tested in C57BL/6 mice at 1 mpk using a 30% propylene glycol/70% PBS vehicle at a concentration of 0.5 mg/mL or at 1 mpk using a 20% DMSO/60% propylene glycol/20% water vehicle at a concentration of 1 mg/mL. All determinations are the average of two mice from a single experiment. The indicated errors are the difference between the mean and the individual values. [b]Compound was tested in Wistar Han rats at 1 mpk using a 20% DMSO/60% PEG/20% water vehicle at a concentration of 1 mg/mL. All determinations are the average of two rats from a single experiment. The indicated errors are the difference between the mean and the individual values. [c]Protein binding values are a single determination.

Scheme 2. Synthesis of Compounds 62−63

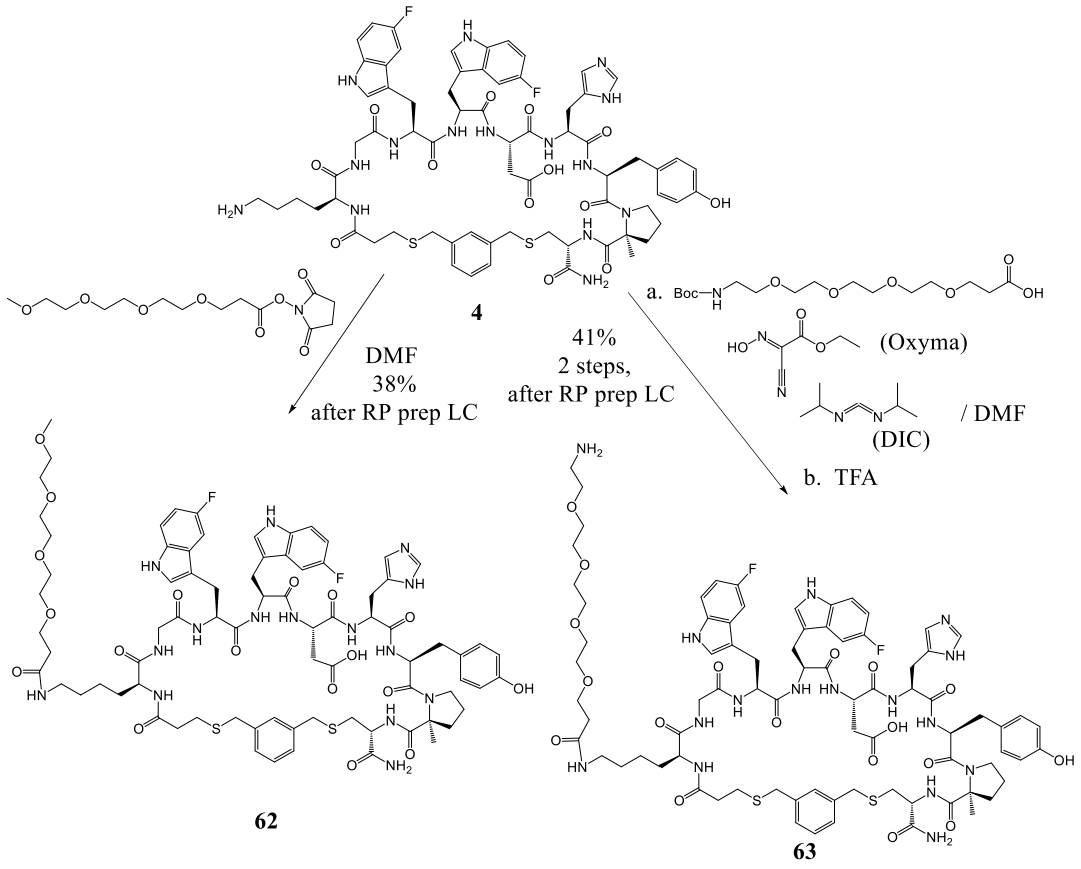

C-terminal amide from this target molecule. We considered a number of possible cross-linking strategies, but a copper-catalyzed alkyne−azide cyclization (Click)[26] reaction between an *N*-propargyl-substituted 5F-Trp and an azido-substituted

https://dx.doi.org/10.1021/acs.jmedchem.0c01084
J. Med. Chem. XXXX, XXX, XXX−XXX

Scheme 3. Synthesis of Compound 66

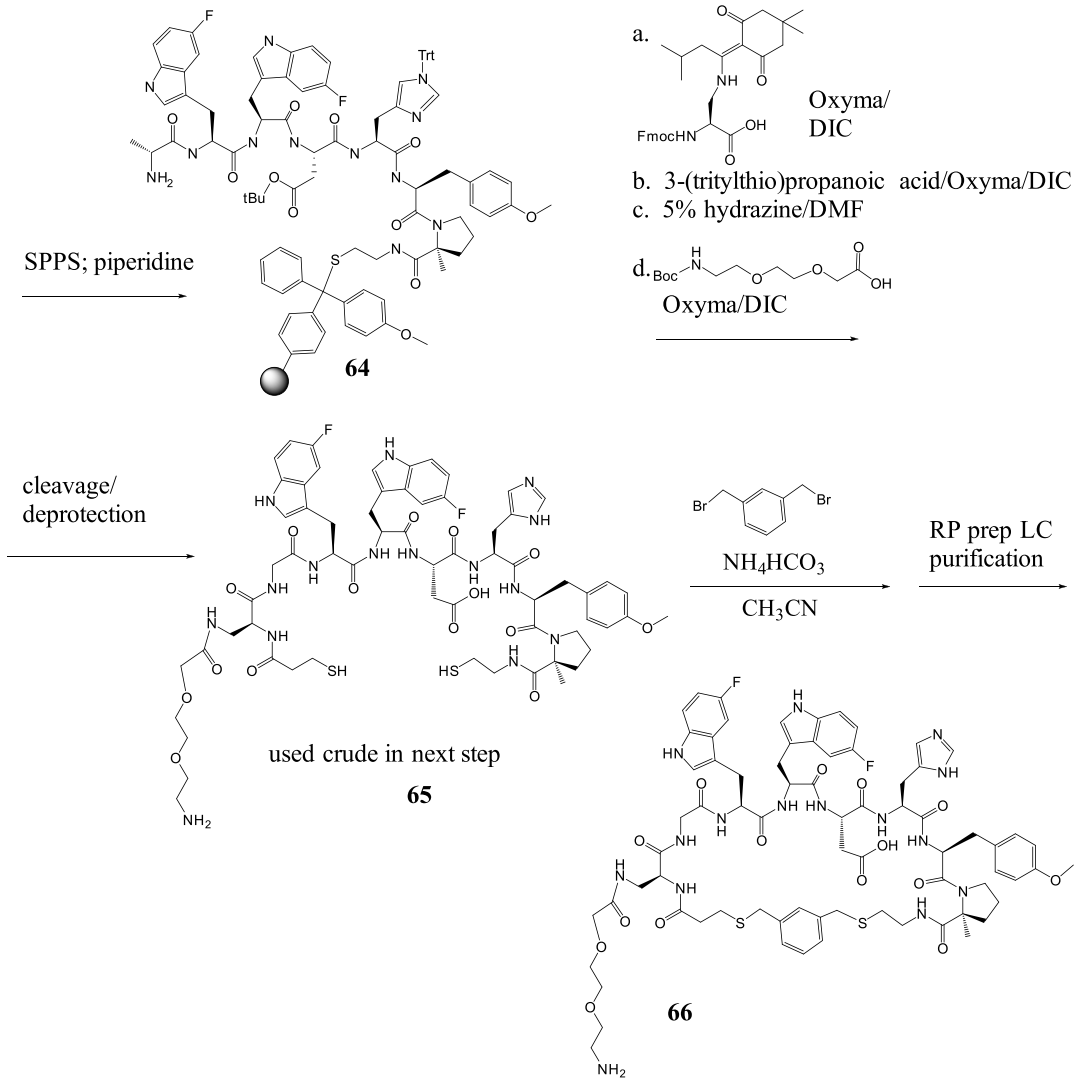

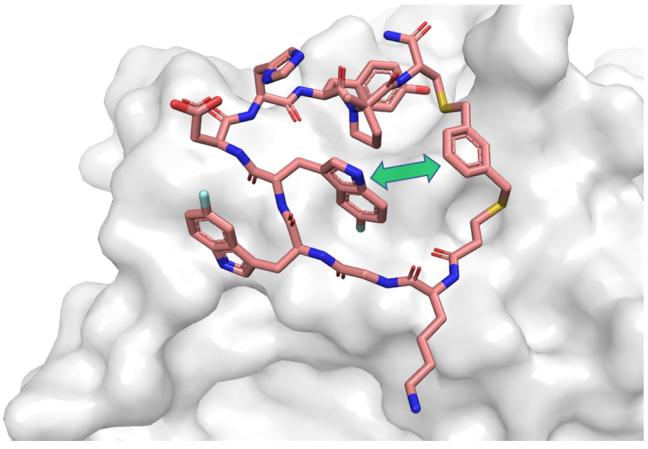

Figure 12. Proposed novel cross-link (green arrow) from bis-meta position of the DBX linker to the indole nitrogen of the 5F Trp in position 4.

linker aryl ring presented an opportunity to bridge the distance with a novel spacer of the appropriate length.[27] This approach (Chart 1)[27] also provided a very synthetically accessible route and the appropriate orthogonality of the associated functional groups to the target molecule. It was necessary to synthesize the requisite *N*-propargyl 5F-Trp amino acid and the azido-modified DBX cross-linker. Scheme 4 details the synthesis of the Fmoc-protected *N*-propargyl 5F-Trp amino acid **70**, starting from the commercially available 5F-Trp amino acid. The four-step synthesis was performed in excellent overall yield to give the desired product, which was used directly in solid-phase synthesis to assemble the linear peptide. The aryl azide intermediate **73** was prepared in two steps from a commercial starting material as shown in Scheme 5. The final peptide was assembled as shown in Scheme 6. The linear peptide was assembled using standard SPPS, and the crude linear peptide cleaved and deprotected. The crude linear peptide intermediate was cyclized under standard conditions using the DBX-azide described above (Scheme 5, **73**) to give **74**, which was then subjected to the second cyclization[26] conditions to provide the novel bicyclic peptide **75**. Compound **75** showed similar potency (Alexa-FRET IC_{50} = 1.36 nM) to earlier analogues in the Asp−His series (such as **30**) and some improvement versus analogues in the Pro−Thr series (such as **51**). The molecule showed excellent stability in our protease panel (Table 2) and was dosed IV to both rats and cynomolgus monkeys (Table 10) to evaluate *in*

https://dx.doi.org/10.1021/acs.jmedchem.0c01084
J. Med. Chem. XXXX, XXX, XXX−XXX

Chart 1. Retrosynthetic Analysis of the Proposed Bicyclic Target Peptide

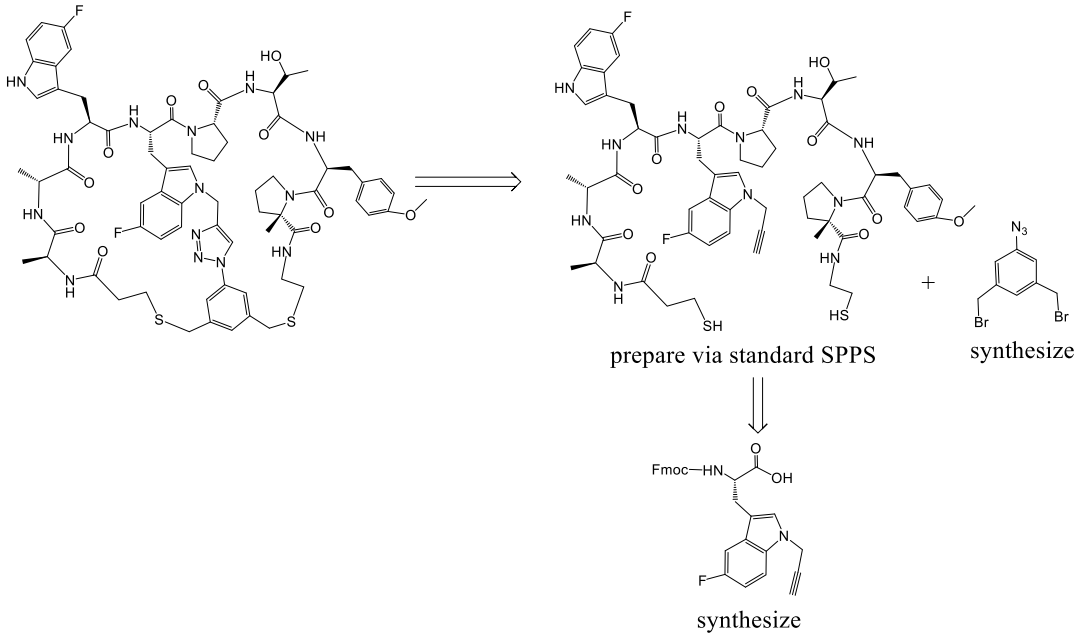

Scheme 4. Synthesis of *N*-Propargyl Fmoc-Protected 5F-Trp 70

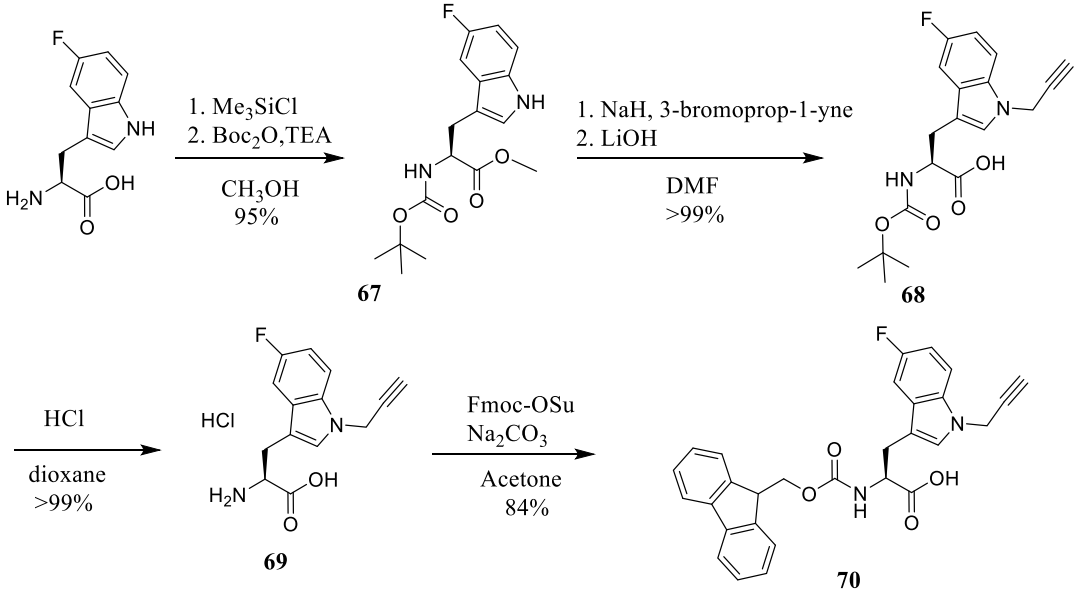

Scheme 5. Synthesis of Arylazide Intermediate 73

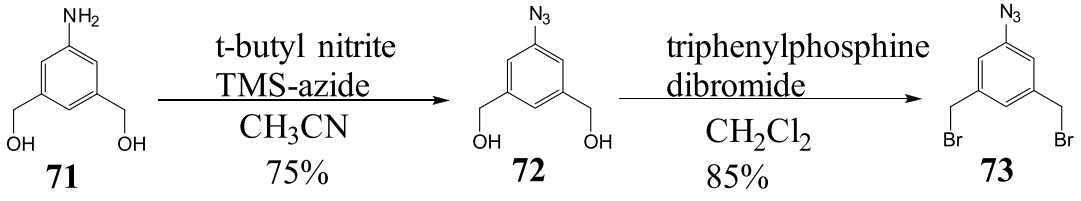

vivo PKs. Interestingly, the compound showed extremely poor IV PK performance in rats; however, it was somewhat better in monkeys, suggesting that the issues seen *in vivo* with molecules containing a Pro at position 5 might be a rodent-specific issue. Despite its poor PK performance in rats, compound **75** represents a key, novel structure in the series, demonstrating good potency, improved stability, and reasonable IV PK performance in cynomolgus monkeys. Unfortunately, we were unable to obtain suitable crystals to allow for determination of a crystal structure of **75**. However, based on the structure shown in Figure 12 as well as the data for **75**, one can deduce that the triazolomethyl linker does not drastically change the overall conformation of the molecule

https://dx.doi.org/10.1021/acs.jmedchem.0c01084
J. Med. Chem. XXXX, XXX, XXX−XXX

Scheme 6. Synthesis of Bicyclic Peptide 75

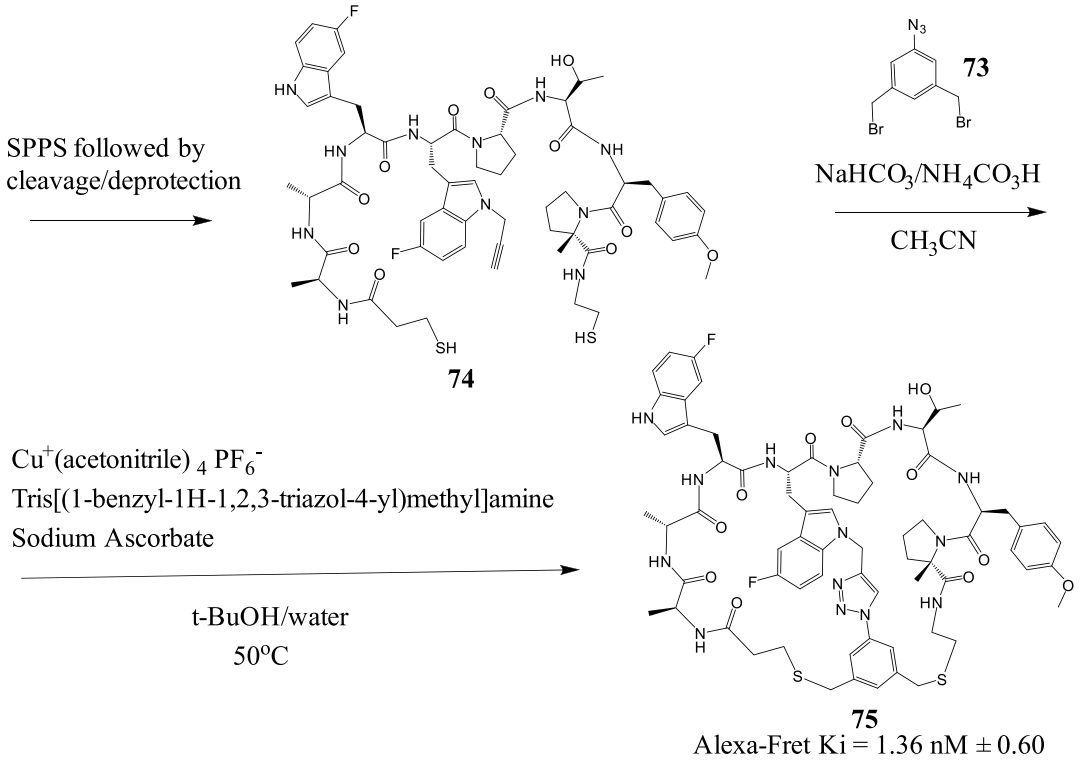

Table 10. Rat and Cyno Monkey IV PKs for 75[a,b,c]

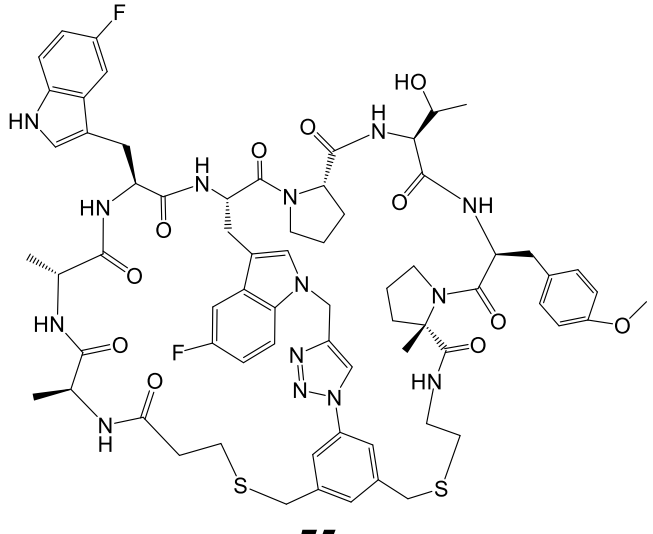

75

species	AUC_{0-inf} (nM h)	AUC_{0-x} (nM h)	clearance (mL/min/kg)	V_{dss} (L/kg)	$T_{1/2}$ (h)	protein binding[c] (% bound)
cynomolgus monkey[a]	306.10 ± 48.85	303.71 ± 49.57	20.15 ± 3.15	1.06 ± 0.13	2.84 ± 1.46	97.5
Wistar Han rat[b]	23.3 ± 4.1	19.4 ± 0.6	107 ± 18	0.48 ± 0.07	0.06 ± 0.02	99.7

[a]Compound was tested in cynomolgus monkeys at 0.5 mpk using a 30% propylene glycol/70% PBS vehicle at a concentration of 0.5 mg/mL. All determinations are the average of two monkeys from a single experiment. The indicated errors are the difference between the mean and the individual values. [b]Compound was tested in Wistar Han rats at 1 mpk using a 20% DMSO/60% PEG/20% water vehicle at a concentration of 1 mg/mL. All determinations are the average of two rats from a single experiment. The indicated errors are the difference between the mean and the individual values. [c]Protein binding values are a single determination.

and likely serves as a simple direct link from the NH of the Trp to the aryl ring of the DBX group.

There was also a second possible cyclization opportunity that became apparent to us from the crystal structures of **30** and **51**. We observed that the indole ring of 5F-Trp at position 3 and the side chain of Asp at position 5 were pointing outward into the solvent and were relatively close to each other. This suggested the possibility of closing a ring between the side chain of the Asp and the aryl ring of the side chain of 5F-Trp, as illustrated in Figure 13. Such a ring could

https://dx.doi.org/10.1021/acs.jmedchem.0c01084
J. Med. Chem. XXXX, XXX, XXX−XXX

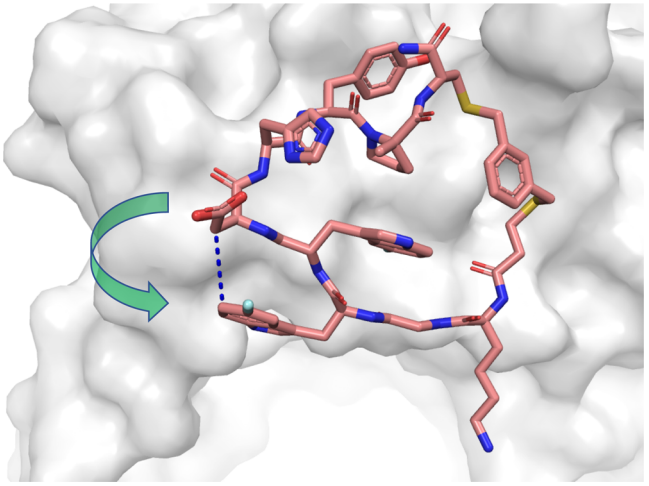

Figure 13. Proposed cyclization between the side chain of position 3 and position 5. The side chains point in the same direction and are in close proximity to each other, and the new bicyclic linker would lie in a mostly solvent-exposed region.

potentially serve to block metabolism at most or all of the remaining vulnerable amide bonds while also helping to lock the conformation of the molecule in its preferred binding conformation, thereby providing potential entropic gains. Of course, this would remove the existing intramolecular interaction between the Asp and His side chains but would constrain the overall conformation in a different manner.

We decided to strip off the side chain of Lys at position 1 to a methyl group for ease of synthesis and to temporarily avoid the mast cell degranulation issue. After scanning the literature and available starting materials, we discovered that the meta-(aminomethyl)phenylalanine was commercially available and decided to use this as a replacement for 5F-Trp in position 3. We could then use amino acids containing carboxylic acid side chains at the Asp position 5 and attempt macrolactamization of these two amino acids to provide an amide cross-linked analogue. Scheme 7 details the synthesis of these lactam cross-linked analogues, and Figure 14 details the SAR progression of the bicyclic series of inhibitors. The linear peptides were prepared on resin, followed by cleavage and deprotection to provide **76**. **76** was then cyclized using meta-dibromomethyl benzene (DBX), and the crude product purified via reversed phase prep HPLC to give the purified macrocycle **77**. The peptide was then treated with the coupling agent AOP[28] in the presence of DIEA to form the cyclic lactam, and the crude material again purified via reverse-phase prep HPLC to give

Scheme 7. Representative Synthesis of Lactam Analogues

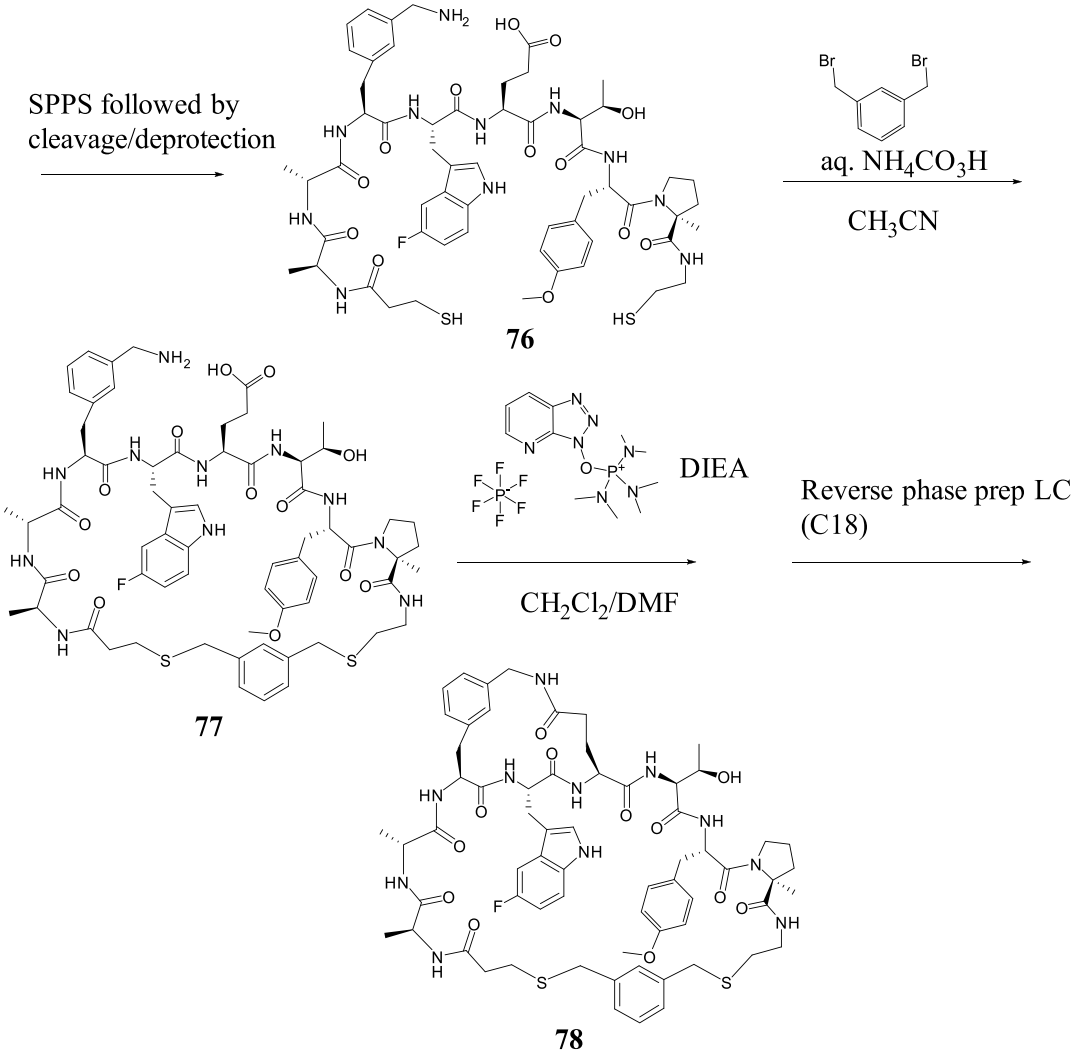

https://dx.doi.org/10.1021/acs.jmedchem.0c01084
J. Med. Chem. XXXX, XXX, XXX−XXX

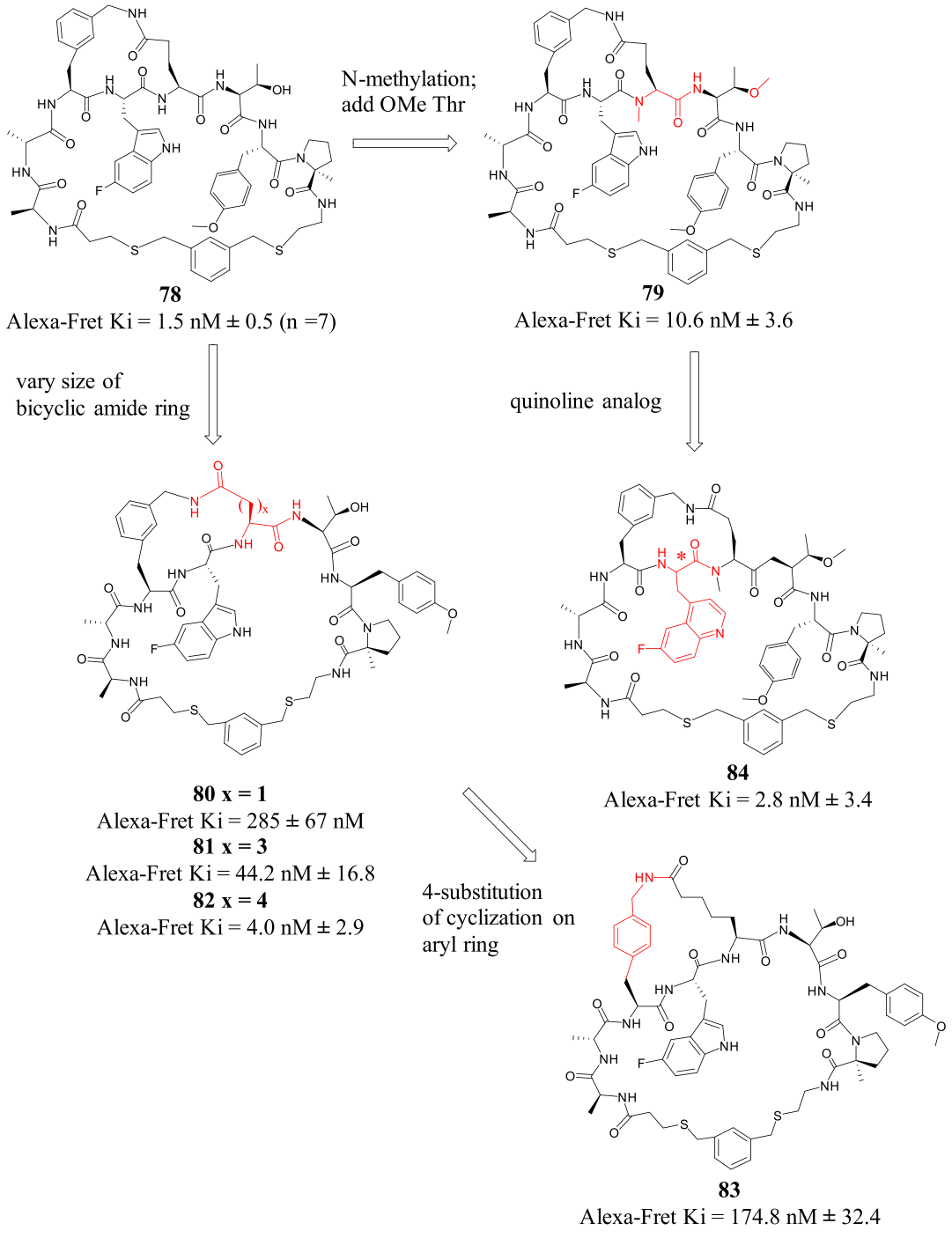

Figure 14. SAR and evolution of bicyclic amide PCSK9 inhibitors.

the desired bicyclic lactam analogue **78**. This general synthetic approach was used to prepare the various amide analogues in this series. Compound **78** showed excellent potency in the LDLR-FRET assay, thus confirming our hypothesis about cyclization in this region. We were able to obtain a crystal structure of **78**, which is detailed in Figures 15 and 16. Other than a slight twist of the DBX cross-linker group (there is some enlargement in the density here, suggesting some mobility for the aryl ring of the DBX cross-linking group), the crystal structure of compound **78** is very similar to the previous crystal structures in this series. Figure 15 shows that the molecule retains all the interactions of the previous inhibitors, with the addition of the lactam bicycle. Figure 16, which shows an overlay of **78** versus **30**, confirms the superimposability of the two structures. The crystal structure also suggests that all the vulnerable amide bonds are now in some way shielded, suggesting the potential for better stability. However, when we looked at the stability of compound **78** in our panel of proteases and in whole blood, we noted that a potential vulnerability to chymotrypsin remained (Table 2). Despite marginal solubility, compound **78** was evaluated for IV PK in the mouse (Table 2), and the compound was shown to have a short half-life *in vivo*. In Figure 15 (highlighted in the black box), one of the amide nitrogen atoms previously identified as being susceptible to proteolysis by chymotrypsin

https://dx.doi.org/10.1021/acs.jmedchem.0c01084
J. Med. Chem. XXXX, XXX, XXX−XXX

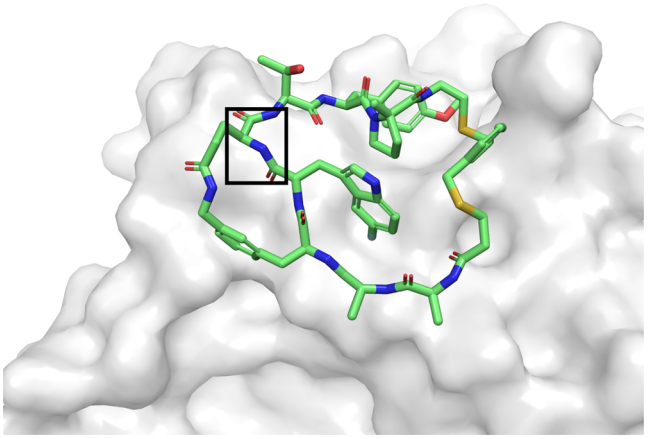

Figure 15. Crystal structure of **78** bound to the LDLR-binding site of PCSK9 at 1.43 Angstrom resolution (PDB: 6XIE). The new bicyclic ring between positions 3 and 5 is clearly visible. The phenylalanine ring at position 3 occupies the same space as the fused ring system of 5F-Trp it replaces. Other than a slight twist of the DBX cross-linker aromatic ring, the rest of the molecule fits in a virtually identical manner to previous crystal structures in this series. The nitrogen of the amide bond between the inner 5F-Trp at position 4 and the glutamic acid at position 5 (indicated by the black box) remains exposed and vulnerable to chymotrypsin (see Table 2). The crystal structure suggests that this nitrogen should be amenable to methylation because it points upward and away from the protein and does not participate in any interactions with the protein.

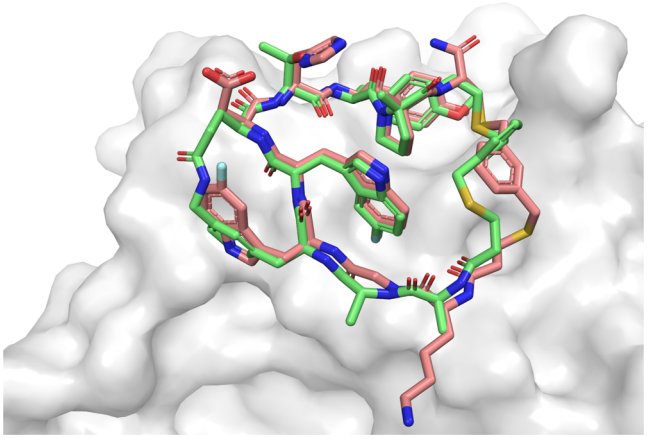

Figure 16. Superposition of the crystal structures of **30** (salmon) and **78** (green). The two molecules bind in a similar fashion, with all of the key hydrogen bonding and lipophilic interactions maintained. There is a slight twist in the DBX cross-linker (extra density here indicates likely some flexibility here). The new ring formed between the side chains of position 3 and position 5 is clearly visible, with the aryl ring sitting in a similar position as the indole of 5F-Trp and the newly formed cyclic amide solvent-exposed.

remains unsubstituted in the structure and despite the presence of the bicycle this remains a vulnerability.

Because this amide bond does not participate in any hydrogen bonding interactions with the protein and points upward and away from the protein, based on the crystal structure, we rationalized that it should be amenable to N-methylation. Our earlier *N*-methyl scan had suggested that N-methylation at this position would not be well tolerated; however, given the somewhat different nature of this bicyclic structure, we decided to attempt N-methylation here. N-Methylation of the amide nitrogen between positions 4 and 5 (synthesized via a procedure identical to the one detailed earlier for **78** but using *N*-Me Glu at position 5 in place of Glu) provided **79**, which demonstrated good potency, although somewhat reduced from that seen with the parent (Figure 14). Note that in going from peptide **78** to **79**, we also introduced an OMe Thr moiety in place of Thr. As stated earlier for compounds **50** versus **52**, we had previously established that Thr and OMe Thr provided identical inhibitory potency and did not affect stability (Table 2), and these amino acids were used interchangeably in several cases. While the comparison between **78** and **79** is not perfectly direct, the change from *N*-H to *N*-Me at this key backbone position clearly provided a stability advantage (Table 2) against chymotrypsin similar to that observed when going from a Asp−His backbone like **30** to a Pro−Thr backbone such as **50**. Compound **79** showed full stability against our panel of proteases as well as in the presence of mouse and cyno monkey whole blood, suggesting that the structure-guided changes we had made in the backbone were able to effectively block potential metabolism by key proteases. This was an important finding for our program and shows that structural information is key in drug discovery programs and can be used to not only enhance potency and drive SAR but also to guide efforts to stabilize metabolically vulnerable functionalities on key structures. Given the extremely poor solubility of compound **79**, we chose not to dose it *in vivo*.

Additional studies were done around compounds **78**−**79** to look at various ring sizes for the lactam bicycle (Figure 14). The peptides were synthesized in an identical manner to **78**, substituting the appropriate amino acids in the SPPS. Contracting the ring by one carbon (Asp at position 5) to give **80** provided a substantial potency loss. Expanding the ring by one carbon versus **78** (homoGlu at position 5) gave **81**, which lost 20-fold in inhibitory potency. Further enlarging the ring by one additional carbon versus **78** (bishomoGlu at position 5) gave **82**, which almost fully restored inhibitory potency. Finally, moving the substitution pattern of the aminomethyl group on the phenylalanine ring at position 2 from meta to para and cyclizing with the lengthened bishomoGlu used in analogue **82** provided **83**, which lost about 100-fold in potency but still retained somewhat interesting activity. We also continued to look for replacements for the 5F-Trp moiety in position 4 that bound inside the macrocycle with the fluorine embedded in a small pocket on the surface of the binding site. We were able to purchase the racemic 5F-4-quinoline amino acid, and synthesis of the peptide using this amino acid gave **84** (Figure 14), which was isolated as an approximately 1:2 mixture of isomers at the quinoline amino acid center after chromatography and was tested as a mixture. The mixture of diastereomers **84** showed a slightly improved potency to the analogous 5F-Trp analogue and represented the only amino acid side chain that we found that was able to duplicate the activity seen with 5F-Trp at this position. We were able to obtain a crystal structure of **84**, shown in Figure 17, overlaid with the crystal structure of **30**. Only the correct diastereomer is able to bind and form suitable crystals and as such is the isomer represented in the crystal structure. The overlay shows that the fluoroquinoline ring of **84** appears to be a fully superimposable replacement for the 5F-Trp moiety of most of the inhibitors. This data once again reaffirmed the narrow SAR observed at this

https://dx.doi.org/10.1021/acs.jmedchem.0c01084
J. Med. Chem. XXXX, XXX, XXX−XXX

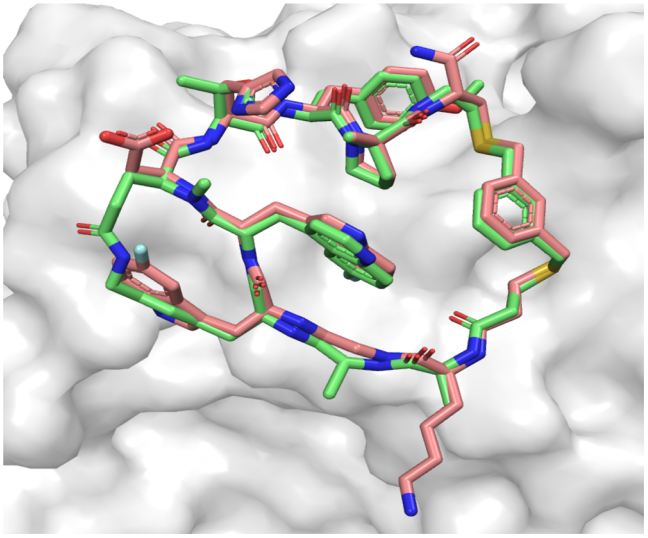

Figure 17. Crystal structure of **84** at 1.77 Angstrom resolution (green; PDB: 6XIF) overlaid with the crystal structure of **30** (salmon) bound to the LDLR binding site of PCSK9. The overall fit of the molecule is identical to all of the previous inhibitor structures described in this publication. The fluoroquinoline at position 4 is shown to occupy the same pocket in an identical manner as 5F-Trp in previous crystal structures.

position and the critical nature of the aryl fluorine substitution here. Based on the combination of the marginal PK demonstrated with **78** as well as the poor solubility in general of these analogues, compounds **80**–**84** were not evaluated *in vivo*.

CONCLUSIONS

In summary, by leveraging a structure-based design approach, we have taken an initial lead from an mRNA display screen and optimized the molecule, increasing the potency by almost 1000-fold, while finding two unique structural approaches to stabilize the molecules to key gut proteases and also reducing the molecular weight by 30%. We have also investigated an observed off-target issue of mast cell degranulation and have developed an SAR to mitigate this issue, which is a potential issue across all peptide platforms and should be suspected when the structural phenotype is present in the molecule or idiosyncratic toxicity is observed. Having optimized potency and stability to key gut enzymes and engineered out an important off-target issue, we are continuing our efforts in this series using these bicyclic platforms as a foundation, with the goal of finding novel, orally bioavailable cyclic peptide PCSK9 inhibitors. Although these novel bicyclic peptide inhibitors are not fully optimized, they provide a novel, potent, and metabolically stable platform for continued lead optimization in this space.

EXPERIMENTAL SECTION

General Methods. Amino acid building blocks and reagents were obtained from various commercial sources such as Sigma-Aldrich, Fisher, Novabiochem, Bachem, Chem-Impex, Iris, Genscript, Frontier, or Nagase & Co. Ltd., WuXi Apptec. The noncanonical amino acid Fmoc-5F-Trp was supplied by WuXi Apptec. SPPS resins were obtained from EMD and Anaspec. The purities of intermediates and final compounds were determined by LC/MS, conditions as follows unless otherwise noted using these methods:

Method A—Waters Acquity BEH C18 column (2.1 × 100 mm, 1.7 μm) eluting with 0.1% trifluoroacetic acid (TFA) in water (solvent A) and 0.1% TFA in acetonitrile (solvent B) at a flow rate of 0.4 mL/min at 45 °C using a 0–4.0 min:25–45% B, 4.0–4.5 min 80% B gradient, detection via UV @ wavelengths of 215 nm. The mass spectra (MS) were recorded on a Waters ZQ mass spectrometer using the electrospray-positive ionization mode [ES^+ to give $(MH)^+$ molecular ions]. The cone voltage was 20 V.

Method B—Waters Acquity BEH C18 column (2.1 × 100 mm, 1.7 μm) eluting with 0.1% TFA in water (solvent A) and 0.1% TFA in acetonitrile (solvent B) at a flow rate of 0.4 mL/min at 45 °C using a 0–4.0 min:20–40% B, 4.0–4.5 min 80% B. The mass spectra (MS) were recorded on a Waters ZQ mass spectrometer using the electrospray-positive ionization mode [ES^+ to give $(MH)^+$ molecular ions]. The cone voltage was 20 V.

Method C—Waters BEH 130 C18 Acquity 2.1 × 100 mm, 1.7 u column, A/B mobile phases—A = 0.1% TFA in water; B = 0.1% TFA in acetonitrile; flow rate = 0.4 mL/min at 45 °C using a 5–95% B gradient over 10 min; and detection via UV @ wavelengths of 215 nm/254 nm (for some examples, 280 nm also), MS: API-ES. Cone voltage = 20 V.

Method D—Waters Acquity BEH C18 50 mm × 1 mm × 1.7 μm, eluting with 0.05% TFA in water (solvent A) and 0.05% TFA in acetonitrile (solvent B) at a flow rate of 0.3 mL/min, a column temperature of 50 °C; 5–95% B (0.05% TFA) in 2 min. Detection at 215 nm. MS: API-ES. Cone voltage = 20 V.

Method E—Waters BEH 130 C18 Acquity 2.1 × 100 mm, 1.7 u column, A/B mobile phases—A = 0.1% TFA in water; B = 0.1% TFA in acetonitrile; flow rate = 0.4 mL/min at 45 °C using a 5–95% B gradient over 15 min; detection via UV @ wavelengths of 215 nm/254 nm; the mass spectra were recorded on a Waters ZQ mass spectrometer using the electrospray-positive ionization mode [ES^+ to give $(MH)^+$ molecular ions]. The cone voltage was 20 V.

Method F—Phenomenex EV C18 2.1 × 100 mm, 1.7 u; A/B mobile phases—A = 0.1% TFA in water; B = 0.1% TFA in acetonitrile; flow rate = 0.4 mL/min at 45 °C using a 20–65% B gradient over 6 min. The mass spectra were recorded on a Waters ZQ mass spectrometer using the electrospray-positive ionization mode [ES^+ to give $(MH)^+$ molecular ions]. The cone voltage was 20 V.

Preparative HPLC was performed as indicated below. LC/MS data for all final compounds is summarized in Table 11. The purities of all final compounds were 95% or greater unless otherwise noted. ^1H NMR spectra were recorded in various solvents at ambient temperature using a Varian 600 MHz NMR.

LDLR-FRET Assay. A time-resolved fluorescence resonance energy (TR-FRET) assay was used to measure inhibition of PCSK9-LDLR PPI. Briefly, 20 nM avitag-biotinylated human PCSK9 was incubated with 20 nM His-tagged human LDLR EGFa domain in the presence of 5 nM LANCE Ulight Streptavidin (PerkinElmer) and 5 nM europium-Anti-6xHis (Perkin Elmer) for 2 h covered at room temperature in buffer containing 50 mM HEPES, 150 mM NaCl, 5 mM $CaCl_2$, 0.01% BSA, and 0.01% surfactant P20. Compounds were tested in dose–response and concentrations giving half-maximal inhibition calculated using a four-parameter fit equation. Dose–response curves consisted of 10-point, half-log dilutions over a concentration range from 0.0015532 to 48.8 μM. The goodness of fit for IC_{50} is a four-parameter logistic fit based on the Levenberg–Marquardt algorithm. K_i was then calculated from the IC_{50} and K_D of PCSK9 to LDLR (480 nM, determined by SPR). The number of replicates varies for the compounds, and full details are provided in the table footnotes. For determinations of $n < 3$, the error is characterized as the difference between the individual values and the mean. For determinations of $n = 3$ or greater, the error is characterized as the standard deviation. All n values are the result of independent determinations.

Alexa-FRET Assay. The PCSK9 TR-FRET Alexa-FRET Standard assay measures the interaction between PCSK9 (biotinylated/C-Avitagged) and an AlexaFluor647 (AF)-tagged cyclic peptide, reagent A (K_D = 83 nM). A solution containing 1 nM biotinylated PCSK9 +

https://dx.doi.org/10.1021/acs.jmedchem.0c01084
J. Med. Chem. XXXX, XXX, XXX–XXX

Table 11. Tabulated LC/MS Data for All Final Molecules[a,b]

compound #	MW	MS $[M + H]^+$	MS $[M + 2H]^+$	LC method	t_R (min)
2	1890.14		945.3	A	2.64
3	1475.67	1476.6		C	3.54
4	1418.62	1419.4		C	3.7
5	1359.48	1360.7	681.1	A	3.38
6	1429.6	1431.2	716.1	A	2.61
7	1282.5	1283.9	642.6	A	2.79
8	1283.45	1284	642.8	A	2.47
9	1371.6	1372.9	687.1	A	2.51
10	1350.51	1351.6	676.1	A	3.18
11	1323.5	1324.9	663.1	A	2.31
12	1390.54	1391.5	696.2	A	2.34
13	1416.57	1417.8	709.2	A	2.5
14	1398.57	1399	700.1	A	2.54
15	1398.57	1398.8	700.3	B	3.67
16	1416.57	1417.3	709.6	B	4.07
17	1416.57	1417	709.6	A	2.56
18	1416.57	1417.7	709.1	A	2.78
19	1416.57	1416.9	709.4	A	3.04
20	1416.57	1417	709.1	A	2.42
21	1430.6	1431.0	716.4	A	2.29
22	1430.6	1431.1	716.2	A	2.5
23a	1412.63	1413.2	707.3	B	3.67
23b	1412.63	1413.4	707.3	B	3.67
24a	1412.63	1413.1	707.1	A	2.51
24b	1412.63	1413.1	707.4	A	2.56
25	1430.62	1432	716.1	A	2.77
26	1430.6	1431.1	716.3	A	2.76
27	1430.62	1431.1	716.3	A	2.7
28	1431.64	1432.7	716.7	A	2.83
29	1372.53	1372.2		C	4.15
30	1429.55	1429.2		C	3.84
31	1454.57	1454.2		C	3.5
32	1454.57	1454.2		C	3.52
33	1408.55	1408.2		C	4.04
34	1434.57	1434.2		C	4.42
35	1374.61			C	3.64
36	1390.5	1390.9	969.1	A	3.4
37	1401.52	1401.2		C	4.04
38	1429.55	1429.2		C	4.04
39	1388.62	1389.6		C	4.25
40	1402.64	1403.6		C	4.91
41	1461.6	1462	732	D	0.82
42	1416.6	1417.6		C	3.06
43	1444.72	1445.7		C	5.29
44	1444.72	1445.7		C	5.3
45	1445.59	1446.6		C	4.98
46	1414.6	1415.7		C	4.53
47	1468.7	1469.2		C	5.23
48	1456.7	1457.7		C	5.4
49	1332.57	1333.5		C	4.9
50	1376.62		688.31	D	0.85
51	1407.6	1408.8		D	0.98
52	1390.65	1391.9		D	0.95
53	1408.64	410		D	0.98
54	1402.58		701.9	C	5.38
55	1416.57	1417.8	708	D	0.66
56	1401.59	1402.8	701.4	D	0.94
57	1415.6	1416.6		C	5.77
58	1430.63	1431.1		C	5.26
59	1443.6	1444.1		C	5.38
60	1457.7	1457.64 (M^+)		E	4.52
61	1441.7	1442.61		E	4.75
62	1647.7		825.4	E	4.8
63	1676.7		839.6	C	4.63
66	1517.61	1518.3		E	4.7
75	1383.62	1383.8		C	6.33
78	1290.56	1291.2		C	5.31
79	1317.6	1318.2		C	6.2
80	1276.6	1277.1		C	5.29
81	1304.58	1305.1		C	5.3
82	1318.61	1319.2		C	5.32
83	1317.6		659.5	C	5.28
84[b]	1328.6	1329.57		F	3.90, 4.11

[a]LC methods are described in the Experimental Section; all molecules demonstrated >95% purity by LC; representative LC traces for key molecules are provided in the Supporting Information. [b]Compound **84** was recovered as a mixture of diastereomers, combined purity > 99%; MS for each peak was identical.

2.5 nM Lance Streptavidin Europium (Strep-Eu) was made in 50 mM HEPES pH 7.4, 0.15 M NaCl, 5 mM $CaCl_2$, 0.01% BSA, and 0.01% surfactant P20. A separate solution containing 40 nM of the AlexaFluor-tagged cyclic peptide was made in the same buffer system. An Echo robot was used to transfer 0.750 μL of test compound to an assay plate, followed by the addition of 15 μL of PCSK9+Stept-Eu and 15 μL of AF peptide. The final assay volume was 30.750 μL containing 0.5 nM PCSK9, 1.25 nM Strep-Eu, and 20 nM AF cyclic peptide. The reaction was incubated at room temperature for at least 2 h prior to fluorescence measurements using an Envision Multilabel Reader. IC_{50} values were determined by fitting data to a sigmoidal dose−response curve using nonlinear regression. Compounds were tested in dose−response and concentrations giving half-maximal inhibition were calculated using a four-parameter fit equation. The dose−response curves consisted of 10-point, half-log dilutions over a concentration range from 0.0015532 to 48.8 μM. The goodness of fit for IC_{50} is a four-parameter logistic fit based on the Levenberg−Marquardt algorithm. K_i was then calculated from the IC_{50} and K_D of the AF cyclic peptide. Counts (B-counts) of the europium-labeled PCSK9 were followed to observe if compounds were adversely affecting PCSK9. A fall-off of the B-counts likely indicated a false positive of inhibition. The number of replicates varies for the compounds, and full details are provided in the table footnotes. For determinations of $n < 3$, the error is characterized as the difference between the individual values and the mean. For determinations of $n = 3$ or greater, the error is characterized as the standard deviation. All n values are the result of independent determinations.

Reagent A was prepared as shown below:

Synthesis of reagent A: compound **30** (15 mg) was dissolved in 0.2 mL of dry DMSO. Then, 15 mg of AlexaFluor 647NHS Ester (A37566, Life Technology) dissolved in 1.5 mL of dry DMSO was added. Dry DIEA (20 μL) was added. The reaction was left under stirring at room temperature for 12 h under the nitrogen atmosphere in the dark, quenched with TFA (pH to 3−4), and purified by RP-HPLC (Dr Maish, Reprosil Gold C18, 250 × 20 mm, 120 c5, 10 μm; 20 to 35% of 0.1% TFA in ACN/0.1% TFA in H_2O, over 20 min, then 35 to 40% over 5 min at 20 mL/min flow rate). The collected fractions were lyophilized to afford 16.1 mg of purified reagent A. LCMS analysis was calcd for $C_{105}H_{122}F_2N_{17}O_{26}S_6^{3-}$, calc. 2268.58; found 1135.8 $[M + 2H]^+$.

https://dx.doi.org/10.1021/acs.jmedchem.0c01084
J. Med. Chem. XXXX, XXX, XXX−XXX

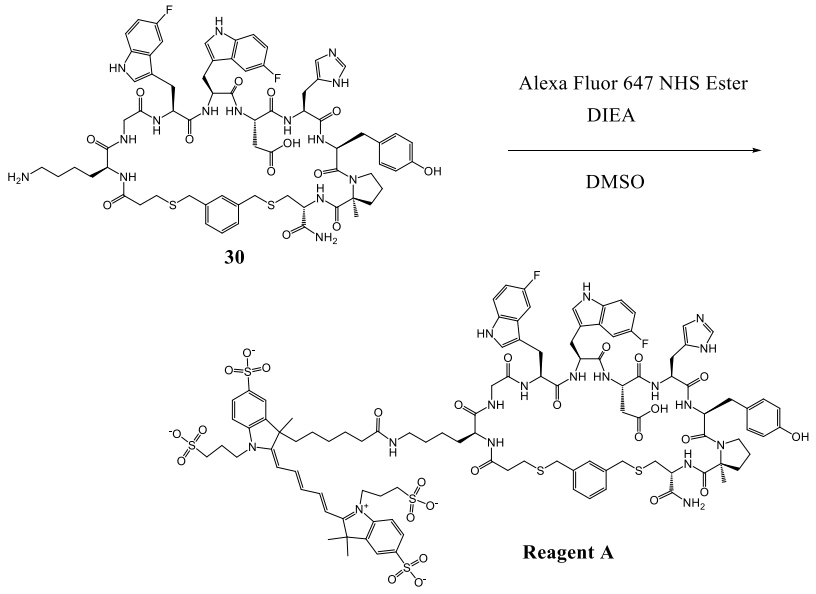

General Procedure for the Preparation of Peptides 2−61. Methods A and B below were used interchangeably with similar results obtained from each. In general, the yields of final peptides **2-61** varied from 5 to 50% after SPPS, cleavage, cyclization, and purification, and in all cases, the desired products were recovered after purification in >95% purity. In the cases of compounds **41** and **51**, the commercially available 1,3-di(bromomethyl)-5-fluorobenzene was substituted for 1,3-di(bromomethyl)benzene (DBX) in step 3 (cyclization) using identical conditions.

Method A. Step 1: Peptide Synthesis. The peptides were synthesized using commercial Fmoc-protected amino acids on a solid-phase Rink Amide MBHA (NovaBiochem, ∼0.5 mequiv/g, 100−200 mesh) or AM (NovaBiochem, ∼0.73 mequiv/g, 100−200 mesh) or 2-aminoethanethiol-2-chlorotrityl resin (Anaspec, ∼0.9 mequiv/g, 200−400 mesh) with a CEM Liberty Blue automated microwave peptide synthesizer. The peptides were typically synthesized on a 0.1 mmol scale. Typical reaction conditions were as follows: deprotection conditions: 20% piperidine (v/v) in dimethylformamide (DMF) (2 × 2 min at 75 °C); residue coupling conditions: 5 equiv (relative to resin) of activated amino acid (2.5 mL of a 0.2 M amino acid stock solution in DMF) was delivered to the resin, followed by 5 equiv of DIC activator (1 mL of a 0.5 M solution in DMF) and 5 equiv of Oxyma Pure (0.5 mL of a 1 M solution in DMF) and allowed to react for 5 min at 75 °C. The resultant product was used directly in the next step.

Step 2: Cleavage from Solid Support. The resin from step 1 was transferred to either a 50 mL polypropylene centrifuge tube or a 10 mL fritted syringe. The peptides were cleaved from their solid support using TFA/triisopropylsilane/DL-dithiothreitol/water (92.5/2.5/2.5 (w/v)/2.5) mixture. For 0.1 mmol scale of resin, ∼10 mL cleavage solution was used. The suspended resin was rocked in cleavage solution for 3 h at room temperature. The filtrate was collected in 50 mL polypropylene centrifuge tubes and precipitated with chilled diethyl ether (∼50 mL per ∼5 mL cleavage filtrate). The precipitated crude peptide was collected by centrifugation. The white pellet was then subsequently suspended in chilled diethyl ether and collected by centrifugation two additional times. The resulting solid was air-dried to afford the crude peptide.

Step 3: Cyclization. For a 0.1 mmol scale, the linear peptide was synthesized, cleaved from the solid support, and isolated according to step 2. The solid crude peptide was dissolved with stirring in 30 mL of a degassed water/acetonitrile (1:1) solution in a 50 mL polypropylene centrifuge tube. Additional acetonitrile was added as needed to ensure complete dissolution of the peptide. To this stirred solution, aqueous ammonium bicarbonate (200 mM, degassed) was added dropwise to bring the pH to ∼8. Alkylating reagent 1,3-di(bromomethyl)benzene (0.1 mmol/1 equiv) in acetonitrile (1 mL) was added dropwise to the reaction over ∼2 min. After complete addition, the reaction was tested to ensure that the pH was maintained at ∼8. If the pH was below ∼8, additional aqueous ammonium bicarbonate (200 mM, degassed) was added dropwise to the reaction until the pH was ∼8. The centrifuge tube was capped and the resulting reaction mixture was stirred at room temperature for 1 h. The reaction was then acidified to pH ∼1 with TFA and lyophilized to afford the crude cyclic peptide as a powder. The residue was redissolved in 19:1 DMSO−water (v/v) and purified using gradient elution on reverse phase (50 × 250 mm Sunfire Prep C18; 25−75% CH_3CN/water w/0.1% TFA modifier over 30 min). The fractions were then concentrated *in vacuo* to provide the cyclized peptide.

Method B: Alternative HATU Method on CEM Liberty. Step 1: Peptide Synthesis. The peptide was synthesized using Fmoc/*t*-Bu chemistry on cysteamine 4-methoxytrityl resin (NovaBioChem, 0.82 mmol/g) with a CEM Liberty automated microwave peptide synthesizer. The peptide sequence was typically synthesized on a 0.25 mmol scale. Typical reaction conditions were as follows: Fmoc deprotections were performed using 20% (v/v) piperidine in DMF (10 mL, 90 s at 90 °C). Residue coupling conditions: single couplings of 4 equiv (relative to resin) of Fmoc-protected amino acids (as a 0.2 M DMF solution) along with 3.6 equiv of HATU (as a 0.45 M DMF solution) and 8 equiv of 2 M DIEA in NMP. Coupling cycle: 300 s at 75 °C or for trityl side chain-protected residues: 120 s at 20 °C, followed by 240 s at 50 °C.

Step 2: Cleavage from Solid Support. After isolation of the resin via filtration, the peptide was cleaved from solid support using 15 mL of TFA solution (v/v) (90.5% TFA:2.5% DODT:2.5% phenol:2% triisopropylsilane:2.5% water) for approximately 4 h at room temperature. The resin was filtered and washed with 5 mL of TFA solution. Combined filtrate was concentrated and precipitated in approximately 60 mL of cold ethyl ether (−78 °C). Crude peptide pellet collected by centrifugation was washed in cold ethyl ether and collected by centrifugation twice more. The resulting solid was air-dried to afford the crude peptide.

Step 3: Cyclization. Crude linear peptide (0.25 mmol) was redissolved in a solution of degassed acetonitrile (150 mL) and degassed 20 mM aqueous solution of ammonium carbonate (63 mL, 1.26 mmol), a degassed solution of 1,3-di(bromomethyl)benzene (78 mg, 0.29 mmol) in ACN (5 mL total with rinse) was added, and the reaction under an atmosphere of nitrogen for 18 h was stirred. The reaction was filtered and then concentrated *in vacuo*. The residue was redissolved in 19:1 DMSO−water and purified using gradient elution on reverse phase (50 × 250 mm Sunfire Prep C18; 25−75% CH_3CN/water w/0.1% TFA modifier over 30 min). The fractions were then concentrated *in vacuo* to provide the cyclized peptide.

https://dx.doi.org/10.1021/acs.jmedchem.0c01084
J. Med. Chem. XXXX, XXX, XXX−XXX

Synthesis of Compound 62 (Scheme 2). Compound **4** (4.4 mg, 3.08 μmol) was dissolved in 1.0 mL of DMF. 2,5-Dioxopyrrolidin-1-yl 2,5,8,11-tetraoxatetradecan-14-oate (2.2 mg, 6.60 μmol) was dissolved in 100 μL of DMF and then was added directly to the peptide solution. The reaction was stirred at room temperature for 2 h, at which time LCMS showed the reaction was completed. The reaction mixture was diluted with DMF and water to 3 mL, then purified on RP-HPLC using a Vydac protein & peptide C18, 250 × 10 mm, wide pore; gradient: 20−60% over 50 min.; mobile phases: A = 0.1% TFA in water; B = 0.1% TFA in acetonitrile. Compound **62** (1.90 mg) was obtained with purity >95% (HPLC), calcd $C_{79}H_{99}F_2N_{15}O_{18}S_2$, 1647.67; observed mass $[M + 2H]^+$.

Synthesis of Compound 63 (Scheme 2). Compound **4** (12 mg, 8.39 μmol) was dissolved in 0.5 mL of DMF. 2,2-Dimethyl-4-oxo-3,8,11,14,17-pentaoxa-5-azaicosan-20-oic acid (6.13 mg, 0.017 mmol), (*E*)-ethyl-2-cyano-2-(hydroxyimino)acetate (Oxyma Pure; 0.017 mL, 0.017 mmol), and *N*,*N*′-methanediylidenebis (propan-2-amine) (DIC; 0.034 mL, 0.017 mmol) were mixed together, allowed to stand at room temperature for 30 min. Then, this mixture was added to the peptide solution. LCMS showed the reaction was ongoing. Preactivated Boc-PEG-COOH (0.017 mmol) was added twice to the solution. After 48 h, the reaction was completed by LCMS analysis. The reaction was concentrated, and 2 mL of 1:1 TFA in DCM was added directly to the residue. After 30 min, the TFA solution was concentrated and suspended in cold diethyl ether. The mixture was centrifuged, the precipitate was dissolved in acetonitrile/water, and the solution was freeze-dried to a fluffy white material. Purification was done with RP_HPLC using a Vydac protein & peptide C18, 250 × 10 mm, wide pore, with a 20−60% A gradient over 50 min; mobile phases: A = 0.1% TFA in water; B = 0.1% TFA in acetonitrile.

Compound **63** (5.72 mg) was obtained with purity > 95% (HPLC), calc. $C_{80}H_{102}F_2N_{16}O_{18}S_2$ 1676.70; observed $[M + 2H]^+$ = 839.64.

Synthesis of Compound 66 (Scheme 3). *Step 1—Synthesis of Compound 64.* The peptidyl resin intermediate was synthesized using Fmoc/*t*-Bu chemistry on cysteamine 4-methoxytrityl resin (Novabiochem, 0.82 mmol/g) with a CEM Liberty automated microwave peptide synthesizer. The peptide sequence was synthesized on a 1.0 mmol scale using single couplings of 3.3 equiv of Fmoc-protected amino acids as a 0.2 M DMF solution along with 3.0 equiv of HATU as a 0.45 M DMF solution and 6.6 equiv of 2 M DIEA in NMP. Fmoc deprotections were performed using 20% (v/v) piperidine in DMF.

Compound **64** was sampled for cleavage in 2 mL of 88% TFA, 5% DODT (3,6-dioxa-1,8-octanedithiol), 2% phenol, 2.5% triisopropylsilane, and 2.5% water to check the peptide quality. The correct linear peptide **64** was confirmed. **64** was used as the starting resin in the next step. LCMS anal calcd for $C_{53}H_{62}F_2N_{12}O_{10}S$, 1096.44; found, 1097.0 $[M+H]^+$.

Step 2—Synthesis of Compound 65. Synthesis of linear peptide was continued on **64** (0.1 mmol) on a Biotage Alstra peptide synthesizer (BiotageCorp.) with two cycles of elongation using 4 equiv of double coupling with DIC/Oxyma Pure as activators, and the amino acids (*S*)-2-((((9*H*-fluoren-9-yl)methoxy)carbonyl)-amino)-3-((1-(4,4-dimethyl-2,6-dioxocyclohexylidene)-3-methylbutyl)amino)propanoic acid and 3-(tritylthio)propanoic acid, respectively. Fmoc deprotections were performed using 20% (v/v) piperidine in DMF.

The peptidyl resin was treated with 5% hydrazine in DMF for 10 min (repeated twice) to remove the side chain protection group ivDde. The peptidyl resin was manually coupled with 4 equiv of 2,2-dimethyl-4-oxo-3,8,11-trioxa-5-azatridecan-13-oic acid (2.000 mL, 0.4 mmol) using DIC/Oxyma Pure for 1 h.

The fully assembled peptide on-resin was cleaved using 10 mL of 88% TFA, 5% DODT (3,6-dioxa-1,8-octanedithiol), 2% phenol, 2.5% triisopropylsilane, and 2.5% water for 2 h at room temperature. Another 5 mL of TFA solution was used to wash the peptidyl resin. After filtering, combined TFA solutions were concentrated *in vacuo*. Approximately 40 mL of chilled diethyl ether was added to the mixture to precipitate the peptide. The crude peptide was collected by centrifugation on a Thermo ST40R at 2900 rpm for 15 min. The pellet was then washed with 40 mL of chilled ether again. The washed peptide pellet was dissolved in 0.1% TFA acetonitrile/water solution and then was lyophilized to dryness. The correct linear peptide **65** was confirmed. **65** was used directly as a crude in the next step reaction.

LCMS anal calcd for $C_{65}H_{83}F_2N_{15}O_{15}S_2$, 1415.56; found m/z^{+2}, 709.08.

Step 3—Synthesis of Compound 66. Crude **65** (0.1 mmol) was redissolved in a solution of degassed acetonitrile (60 mL) and 20 mM NH_4HCO_3 in water (90 mL). To this was slowly added a degassed solution of 1,3-di(bromomethyl)benzene (52.8 mg, 0.2 mmol) in acetonitrile (60 mL total with rinse). The reaction was stirred at room temperature until completed (18 h). The reaction was lyophilized to dryness and then purified using gradient elution on the reverse phase (30 × 150 mm OBD, Waters Xselect CSH130 C18, 5 μm; 31−36% ACN/water w/0.16% TFA modifier over 25 min). The fractions were lyophilized to provide **66** in 96% purity (4.6 mg), along with 1.5 mg of a slightly earlier eluting second product identified as a racemate at an undetermined stereocenter (verified by Alexa-FRET assay = 385 nM).

LCMS anal calcd for $C_{73}H_{89}F_2N_{15}O_{15}S_2$, 1517.61; found, 1517.61.

Synthesis of Compound 75 (Schemes 4−6). *Step 1—Synthesis of Intermediate Compound 67 (Scheme 4).* In a flame-dried flask under an atmosphere of nitrogen, (*S*)-2-amino-3-(5-fluoro-1*H*-indol-3-yl)propanoic acid (10.8 g, 48.6 mmol) was dissolved in anhydrous MeOH (200 mL) and cooled in an ice bath. Trimethylchlorosilane (TMS-Cl) was added (35.6 mL, 279 mmol) dropwise, and the resulting solution was stirred at room temperature overnight. An additional 4 mL of TMS-Cl was added, and the reaction was allowed to stir for an additional 18 h to drive the formation of the desired methyl ester.

The reaction was cooled in an ice bath, and triethylamine (38 mL, 273 mmol) was added to raise the reaction pH to ∼9. A solution of BOC-anhydride (12.98 mL, 55.9 mmol) dissolved in methanol (20 mL) was added, and the reaction was stirred at room temperature. After 1 h, an additional 6 mL of triethylamine was added to make the reaction basic, followed by stirring at room temperature for another hour. The reaction was concentrated *in vacuo* and was partitioned residue between water and ether. The aqueous layer was extracted 3× with ether, and the combined extracts were washed with brine and dried over anhydrous Na_2SO_4. The solution was filtered through a plug of silica gel and concentrated *in vacuo*. The residue was concentrated *in vacuo* to dryness. The resultant crystalline solid was triturated with hexanes 3× to provide **67** (15.5 g, 95%).

LCMS anal calcd for $C_{17}H_{21}FN_2O_4$, 336.4; found, 673.5 $(2M + 1)^+$.

^{1}H NMR (600 MHz, chloroform-*d*): δ 8.08 (s, 1H), 7.27−7.24 (m, 1H) (mixed with $CHCl_3$ peak), 7.17 (d, *J* = 9.4 Hz, 1H), 7.04 (s, 1H), 6.96−6.90 (m, 1H), 5.07 (d, *J* = 7.5 Hz, 1H), 4.65−4.61 (m, 1H), 3.69 (s, 3H), 3.30−3.18 (m, 2H), 1.43 (s, 9H).

Step 2—Synthesis of Intermediate Compound 68 (Scheme 4). In a flame-dried flask under an atmosphere of nitrogen, **67** (1330 mg, 3.95 mmol) was dissolved in anhydrous DMF (30 mL) and the resulting solution was cooled in an ice bath. Sodium hydride (60% disp.) was added (125 mg, 4.94 mmol) portionwise. The mixture was stirred for 20 min at 0 °C until it became a pale-colored solution. 3-Bromoprop-1-yne (80% in xylene) (0.529 mL, 4.74 mmol) was added dropwise, and the resulting solution was stirred at 0 °C for an hour. Aqueous lithium hydroxide (1 M, 6 mL, 6.00 mmol) was added dropwise to the solution and the mixture was stirred at room temperature for 90 min. The solution was quenched with 6 mL of 1 N HCl to adjust the pH ∼3. The mixture was extracted 3× with EtOAc, and the combined organic extracts were dried over anhydrous Na_2SO_4, filtered, and concentrated *in vacuo* to provide **68**, which was used as a crude in the next step (1.425 mg, 100%).

LCMS anal. calcd for $C_{19}H_{21}FN_2O_4$, 360.4; found, 721.5 $(2M + 1)^+$.

https://dx.doi.org/10.1021/acs.jmedchem.0c01084
J. Med. Chem. XXXX, XXX, XXX−XXX

*Step 3—Synthesis of Intermediate Compound **69** (Scheme 4).* Crude **68** (1425 mg, 3.95 mmol) was dissolved in 4 M HCl in dioxane (20 mL, 80 mmol) at room temperature. After 45 min, the reaction was concentrated *in vacuo*. The residue was concentrated twice from ether to form a yellow solid, which was dried *in vacuo* to provide **69**, which was used as a crude in the next step (1173 mg, 100%).

LCMS anal. calcd for $C_{14}H_{13}FN_2O_2$, 260.3; found, 261.2 $(M + 1)^+$.

*Step 4—Synthesis of Intermediate Compound **70** (Scheme 4).* Crude **69** (1173 mg, 3.95 mmol) was dissolved in acetone (30 mL) along with a solution of sodium carbonate (838 mg, 7.91 mmol) in water (60 mL). A solution of Fmoc-OSu (1334 mg, 3.95 mmol) dissolved in 30 mL of acetone was added, and the solution was stirred at room temperature for 1 h. The reaction was acidified by addition of 1 N aq HCl (~11 mL) dropwise to lower pH to ~3. The solution was extracted 3× EtOAc, and the combined organic extracts were washed with brine and dried over anhydrous Na_2SO_4. The solution was filtered, and the filtrate concentrated *in vacuo*. The residue was dissolved in DCM and purified by flash chromatography (120 g SiO_2, 10−80% EtOAc/hexanes). The appropriate fractions were concentrated *in vacuo* to provide **70** (1600 mg, 84%). **70** was used in the assembly of the crude linear peptide **74**.

LCMS anal calcd for $C_{29}H_{23}FN_2O_4$, 482.5; found, 483.3 $(M + 1)^+$.

^{1}H NMR (500 MHz, DMSO-d_6): δ 12.71 (s, 1H), 7.88 (d, J = 7.5 Hz, 2H), 7.74 (d, J = 8.3 Hz, 1H), 7.66 (dd, J = 13.2, 7.5 Hz, 2H), 7.47 (dd, J = 8.9, 4.4 Hz, 1H), 7.44−7.36 (m, 3H), 7.34−7.23 (m, 3H), 7.08−7.00 (m, 1H), 5.08−5.00 (m, 2H), 4.27−4.15 (m, 4H), 3.38 (s, 1H), 3.15 (dd, J = 14.6, 4.6 Hz, 1H), 3.00 (dd, J = 14.6, 9.7 Hz, 1H).

*Step 5—Synthesis of Intermediate Compound **73** (Scheme 5).* Compound **71** (5-amino-1,3-phenylene) dimethanol (3 g, 19.59 mmol) was dissolved in acetonitrile (200 mL) under an atmosphere of nitrogen. The solution was cooled in an ice bath and *tert*-butyl nitrite (3.85 mL, 32.4 mmol) was added dropwise to form an orange solution. After 15 min of stirring at 0 °C, trimethylsilyl azide (2.99 mL, 22.52 mmol) was added dropwise over 5 min. The reaction was warmed to room temperature and stirred for 2 h and then concentrated *in vacuo*. The residue was stirred in 2:1 toluene−ether, filtered with 2:1 toluene−ether and 3:1 toluene−hexane rinses, and dried to provide **72** (2.62 g, 74.7%)

^{1}H NMR (600 MHz, CD_3OD): δ 7.12 (s, 1H); 6.96 (s, 2H); 4.59 (s, 4H).

*Step 6—Synthesis of Intermediate Compound **73** (Scheme 5).* Compound **72** (2.62 g, 14.62 mmol) was partially dissolved in DCM (400 mL) under an atmosphere of nitrogen and cooled in an ice bath. Triphenylphosphine dibromide (14.0 g, 33.2 mmol) was added portionwise over 5 min. The resulting mixture was stirred at room temperature for 90 min and the reaction eventually became a solution. TLC (60% EtOAc/hexanes) analysis at this point indicated that the reaction was not complete. An additional 600 mg of triphenylphosphine dibromide was added and the reaction was stirred for an additional 20 min. The reaction was filtered through a 120 g silica gel column, rinsing with 350 mL DCM. The filtrate was concentrated *in vacuo* and dried to provide **73** as a crystalline tan solid, which was stored in a freezer (3.78 g, 85%).

^{1}H NMR (600 MHz, $CDCl_3$): δ 7.18 (s, 1 H), 6.98 (s, 2 H), 4.43 (s, 4 H).

*Step 7—Synthesis of Compound **75** (Scheme 6).* The linear peptide intermediate **74** was prepared as described above in the General Procedure using Method B, steps 1 and 2 incorporating the above synthesized amino acid **70** at the appropriate point in the peptide sequence. After SPPS and deprotection/cleavage as described in Method B, steps 1 and 2, the crude linear peptide **74** (prepared on 0.25 mmol scale) was cyclized as described in Method B, step 3, using 103 mg (0.34 mmol) of **73** (prepared above). The crude product after lyophilization was used as isolated in the next reaction.

The crude product from the above was dissolved in a solution of 100 mL of *t*-BuOH/50 mL water and the soln. bubbled with N_2. To the solution was added 26.5 mg (0.05 mmol) of tris[(1-benzyl-1*H*-1,2,3-triazol-4-yl)methyl]amine and 49.5 mg (0.25 mmol) of sodium ascorbate, followed by 18.6 mg (0.05 mmol) of tetrakis(acetonitrile)-copper(I) hexafluorophosphate. The reaction was stirred at room temperature, but there was no reaction observed after 90 min. Additional portions of the three reagents were added again, and the reaction was heated at 50 °C. The reaction was complete after 90 min. The precipitate was filtered off and washed with *t*-BuOH and water. The resulting filtrate was concentrated *in vacuo* and resuspended in a mixture of acetonitrile and methanol. The crude material was purified by RP prep LC using a Vydac protein & peptide C18, 250 × 10 mm, wide pore, with a 20−60% A gradient over 50 min; mobile phases: A = 0.1% TFA in water; B = 0.1% TFA in acetonitrile. The product fractions were combined and lyophilized to give the desired product (17.5 mg) **75** as a white amorphous powder. LC/MS purity = >95.5%; LC/MS calcd 1537.81; found, 1538.0 $[M+H]^+$.

General Synthesis of Bicyclic Lactam Analogues (Example for Compound 79). Crude linear peptide (0.25 mmol) was redissolved in a solution of degassed acetonitrile (150 mL) and degassed 20 mM aqueous solution of ammonium carbonate (63 mL, 1.26 mmol). To this solution was added a degassed solution of 1,3-di(bromomethyl)benzene (78 mg, 0.29 mmol) in ACN (5 mL total with rinse). The solution was stirred under an atmosphere of nitrogen for 18 h. The reaction was filtered and then concentrated *in vacuo* to give the crude cyclized peptide. The residue was redissolved in 19:1 DMSO−water and purified using gradient elution on the reverse phase (50 × 250 mm Sunfire Prep C18; 25−75% CH_3CN/water w/0.1% TFA modifier over 30 min). The fractions were then concentrated *in vacuo* to provide the mono-cyclized peptide. To a solution of AOP (19.9 mg, 45 μmol) and DIEA (30 μL, 172 μmol) in DCM (100 mL) was added a solution of the above mono-cyclized peptide (50 mg, 34 μmol) in DMF (6 mL) over 60 min via a syringe pump. The syringe was rinsed with DMF (1.5 mL). The reaction was stirred overnight at room temperature. The reaction was then concentrated *in vacuo* to remove the DCM and the residue was purified using gradient elution on the reverse phase (30 × 150 mm Sunfire Prep OBD C18; 30−75% CH_3CN/water w/0.1% TFA modifier over 20 min). The fractions were lyophilized to provide 21 mg of compound **79** as a white powder. Dimeric lactam product was also recovered as a byproduct.

LCMS: 95.6% purity. RT: 6.23 min (@215 nM on 5−95% ACN−water (0.1% TFA) over 10 min on Sunfire C18) anal. calcd for $C_{67}H_{84}FN_{11}O_{12}S_2$, 1317.6; found, 1318.2 $[M + H]^+$.

Stability and Metabolite ID Studies. The metabolism of various compounds was studied upon incubation with fully activated porcine gastric pepsin, bovine pancreatic trypsin, porcine pancreatic type IV elastase, and bovine pancreatic α-chymotrypsin. All reported data is derived from a single determination.

Pepsin. A 100 μg/mL solution of porcine pepsin was prepared by dissolving lyophilized enzyme in 10 mM aqueous hydrochloric acid (pH 2.0). Incubation mixtures were prepared in duplicate in a 96-well propropylene plate by adding 5.0 μL aliquots of 100 μM substrate in DMSO or DMSO only (no-substrate control) to 45 μL of the 100 μg/mL solution of porcine pepsin in 10 mM aqueous hydrochloric acid (pH 2.0), which had been prewarmed at 37 °C. The reactions were terminated after an incubation time at 37 °C of 60 min by the addition of 2 volumes (100 μL) of acetonitrile containing 4.5 μM of an internal standard peptide. True time zero controls were prepared by adding the stopping solution prior to the addition of the substrate. The plates were then vortex-mixed and centrifuged at 2250*g* for 10 min. A 50 μL volume of the supernatant from each well was added to 300 μL of 50/50 acetonitrile/20% aqueous formic acid. The resulting supernatants were subjected to LC−MS/MS analysis.

Trypsin. A 100 μg/mL solution of bovine pancreatic trypsin was prepared by dissolving lyophilized bovine pancreatic trypsin enzyme (in 100 mM sodium phosphate buffer, pH 7.40). Incubation mixtures were prepared in duplicate in a 96-well polypropylene plate by adding 5.0 μL aliquots of 100 μM substrate in DMSO or DMSO only (no-substrate control) to 45 μL of the 100 μg/mL solution of

https://dx.doi.org/10.1021/acs.jmedchem.0c01084
J. Med. Chem. XXXX, XXX, XXX−XXX

bovine pancreatic trypsin in 100 mM sodium phosphate buffer (pH 7.40), which had been prewarmed at 37 °C. The reactions were terminated after an incubation time of 1 and 6 h at 37 °C by the addition of 2 volumes (100 μL) of acetonitrile (with formic acid) containing an internal standard peptide. True time zero controls were prepared by adding the stopping solution prior to the addition of the substrate. The plates were then vortex-mixed and centrifuged at 2250*g* for 10 min. A 50 μL volume of the supernatant from each well was added to 300 μL of 50/50 acetonitrile/20% aqueous formic acid. The resulting supernatants were subjected to LC−MS/MS analysis.

α-Chymotrypsin. A 100 μg/mL solution of bovine pancreatic α-chymotrypsin was prepared by dissolving lyophilized enzyme in 100 mM sodium phosphate buffer, pH 7.40. Incubation mixtures were prepared in duplicate in a 96-well polypropylene plate by adding 5.0 μL aliquots of 100 μM substrate in DMSO or DMSO only (no-substrate control) to 45 μL of the 100 μg/mL solution of bovine pancreatic α-chymotrypsin in 100 mM sodium phosphate buffer (pH 7.40), which had been prewarmed at 37 °C. The reactions were terminated after an incubation time at 37 °C of 1 and 6 h by the addition of 2 volumes(100 μL) of acetonitrile (with formic acid) containing 4.5 μM of an internal standard peptide. True time zero controls were prepared by adding the stopping solution prior to the addition of the substrate. The plates were then vortex-mixed and centrifuged at 2250*g* for 10 min. A 50 μL volume of the supernatant from each well was added to 300 μL of 50/50 acetonitrile/20% aqueous formic acid. The resulting supernatants were subjected to LC−MS/MS analysis.

Type IV Pancreatic Elastase. A 100 μg/mL solution of porcine type IV pancreatic elastase was prepared by dissolving lyophilized enzyme in 100 mM sodium phosphate buffer, pH 7.40. Incubation mixtures were prepared in duplicate in a 96-well polypropylene plate by adding 5.0 μL aliquots of 100 μM substrate in DMSO or DMSO only (no-substrate control) to 45 μL of the 100 μg/mL solution of porcine type IV pancreatic elastase in 100 mM sodium phosphate buffer (pH 7.40), which had been prewarmed at 37 °C. Reactions were terminated after an incubation time at 37 °C of 1 and 6 h by the addition of 2 volumes (100 μL) of acetonitrile (with formic acid) containing 4.5 μM of an internal standard peptide. True time zero controls were prepared by adding the stopping solution prior to the addition of the substrate. The plates were then vortex-mixed and centrifuged at 2250*g* for 10 min. A 50 μL volume of the supernatant from each well was added to 300 μL of 50/50 acetonitrile/20% aqueous formic acid. The resulting supernatants were subjected to LC−MS/MS analysis.

Metabolic Stability with Mouse and Cynomolgus Monkey Whole Blood. The metabolism of peptide candidates was studied upon incubation with C57BL/6 mouse and cynomolgus monkey whole blood. Incubation mixtures were prepared in duplicate in a 96-well propropylene plate by adding 5.0 μL aliquots of either 100 μM substrate peptide in DMSO or DMSO only (no-substrate control) to 45 μL of whole blood, which had been prewarmed at 37 °C. Incubations were terminated after an incubation time at 37 °C of 1, 2, 4, and 6 h by the addition of 2 volumes (100 μL) of acetonitrile containing 0.1% formic acid and 4.5 μM of an internal standard peptide. True time zero controls were prepared by adding the stopping solution prior to the addition of substrate. Plates were then vortex-mixed and centrifuged at 2250*g* for 10 min. A 30 μL volume of the supernatant from each well was added to 180 μL of 50/50 acetonitrile/20% aqueous formic acid. The resulting supernatants were subjected to LC−MS/MS analysis.

Mouse Protein Binding. The binding of test molecules to plasma proteins was determined by equilibrium dialysis using the HT Dialysis apparatus (HT Dialysis LLC, Gales Ferry, CT). The peptide was added to mouse plasma at a final concentration of 2.5 μM. Phosphate-buffered saline (100 mM, pH 7.4) was added to one side of the dialysis plate and an equal volume of plasma containing peptide was added to the other side of the plate in replicates of six for each drug concentration tested. The dialysis plates were incubated at 37 °C under 5% CO_2 for 4 h. Following the dialysis, 50 μL of plasma and buffer were removed from each dialysis well, a matrix match was added to bring the pre-extracted samples to 50% plasma and 50% buffer, and the analyte was extracted by the addition of 250 μL acetonitrile containing 200 nM of the internal standard mixture (labetalol, imipramine, and diclofenac). The samples were vortex-mixed and centrifuged for 5 min at 3200*g*, and the resulting supernatant fractions were analyzed by LC−MS/MS. The below calculation was used to determine percent bound

$$\% \text{ bound} = [C_p]/[C_b] \times 100$$

where C_b is the postincubation concentration of peptide in the buffer side and C_p is the postincubation concentration in the plasma side.

LC−MS/MS analysis was performed on a LC−MS/MS system equipped with an LEAP autosampler (Leap Technologies, Morrisville, NC) and a Thermo Scientific Dionex Ultimate 3000 RS Pump (Thermo Fisher Scientific, Waltham, MA) interfaced to a Sciex 4500 mass spectrometer (Sciex, Framingham, MA) utilizing an electrospray source operating in the positive ion mode using multiple reaction monitoring. Chromatographic separation was achieved on an Acquity HSS T3 UPLC column 2.1 mm × 50 mm, 1.8 μm (Waters Cat# 186003538, Milford, MA), using a mobile phase consisting of 0.1% formic acid in water (solvent A) and 0.1% formic acid in acetonitrile (solvent B) at a flow rate of 0.75 mL/min. The chromatography was run using a gradient elution as follows: the column was equilibrated at 5% solvent B; after sample injection, the gradient was held at 5% solvent B for 0.5 min. Solvent B was then increased to 95% over a 1.5 min period. Solvent B was then maintained at 95% for 0.42 min before it was returned to the initial conditions for 0.83 min. The total run time was 3.25 min.

Crystallography. PCSK9 lacking the C-terminal domain (PCSK9-ΔCRD) was produced and purified as described.[12] The final S60 gel filtration was performed in 20 mM Tris pH 8.0, 300 mM NaCl, 100 mM $CaCl_2$, and 5% glycerol. Fractions containing PCSK9-ΔCRD were combined, concentrated to 12 mg/mL, and frozen in 50 mL aliquots till further use. Peptides were dissolved in DMSO at 100 mM and added with a 2-fold molar excess to PCSK9-ΔCRD. Complexes were incubated for 1 h on ice and screened against commercially available crystallization screens. Suitable crystals appeared with 20% PEG3350, 200 mM $CaCl_2$, and 100 mM MES at pH 6 as the precipitant. Crystals were harvested and cryoprotected with an additional 10% glycerol. X-ray diffraction data were collected at IMCA beamline ID17 and processed using the Globalphasing[29] and CCP4[30] packages. Structures were solved by molecular replacement using 4NMX[12] and refined using BUSTER[29] and Coot.[31] Peptides were modeled using standard amino acid residue definitions or restrains generated using Flynn.[32] Coordinates and experimental data are available from the Protein Data Bank with the accession codes: compound **30**, 6XIB; compound **40**, 6XIC; compound **51**, 6XID; compound **78**, 6XIE; and compound **84**, 6XIF. Authors will release the atomic coordinates and experimental data upon article publication.

Rat Mast Cell Degranulation Assay. Isolation of rat peritoneal lavage was conducted as described in the literature. In brief, Wistar Han rats (males or females) were anesthetized with xylene. About 10 mL of Tyrode buffer (12 mM $NaHCO_3$, 127 mM NaCl, 5 mM KCl, 0.5 mM NaH_2PO_4, 1 mM $MgCl_2$, 5 mM glucose, and 10 mM HEPES, pH 7.4) was injected into the peritoneal cavity, followed by gentle abdominal massage for 30 s. Peritoneal lavage was then collected and centrifuged at 350*g* for 10 min. After discarding the supernatant, the cells are resuspended in Tyrode buffer to achieve a final concentration of 1×10^6 cells/mL. For peptide treatment, 100 μL of freshly isolated rat peritoneal cells was added to a tissue-culture treated 96-well plate. Cells were incubated with either positive control (48/80; used to confirm assay responsiveness)[33] or a titrating concentration of various peptides for 30 min at 37 °C. After incubation, the plate was centrifuged at 350*g* for 2 min at room temperature. The supernatants were collected for histamine measurement and cell pellets are resuspended in Tyrode buffer for cell viability analysis. Histamine and cell viability were measured using the commercially available kits, following vendor's instructions. The amount of histamine in the supernatant was presented as ng/mL, and

https://dx.doi.org/10.1021/acs.jmedchem.0c01084
J. Med. Chem. XXXX, XXX, XXX−XXX

cell viability was presented as percent viable cells compared to vehicle-treated cells. Data were reported in for two determinations, both of which were in close agreement in all cases.

PK Studies. All PK studies in preclinical species were conducted according to the highest ethical standards in accordance with and using procedures approved by the Institutional Animal Care and Use Committee of Merck and Co., Inc., West Point, PA, USA.

Male C57BL/6 mice and male Wistar Hannover rats (n = 2−3 in each arm) were used for IV PK studies. Mice and rats were allowed to fast overnight prior to dosing and fed 2 h postdose. Dual jugular vein and carotid artery surgically cannulated mice or rats were used for dose administration and blood sampling, respectively. Blood samples were collected using an automated blood sampling system (Instech, Plymouth Meeting, PA) after IV administration. All blood samples were collected in EDTA-coated tubes at predose, 0.08, 0.25, 0.5, 1, 2, 4, 7, 12, 18, and 24 h following IV dose administration. Rat blood samples were centrifuged, and the supernatant plasma samples were stored at −70 °C until bioanalysis. In mouse studies, whole blood was diluted with citrate anticoagulant and whole blood PK rather than plasma PK was measured.

Male cynomolgus monkeys (n = 2 per group) weighing 5−10 kg were dosed IV. Monkeys were allowed to fast prior to dosing and fed 2−4 h postdose. IV dose was administered as a bolus via the cephalic or saphenous vein. Blood samples were collected serially from the saphenous, femoral, or cephalic veins in EDTA-coated tubes at predose, 0.08, 0.25, 0.5, 1, 2, 4, 6, 24, 48, and 72 h. All blood samples were centrifuged and the supernatant plasma samples were stored at 70 °C until bioanalysis.

Concentrations in mouse whole blood, rat plasma, and monkey plasma were determined by LC−MS/MS assays following a protein precipitation step. Aliquots (50 μL) of plasma were precipitated by addition of 200 μL of methanol/acetonitrile (80:20) containing a related macrocyclic peptide as an internal standard, followed by centrifugation at 4000 rpm for 5 min. A 200 μL aliquot of the supernatant was transferred into a 96-well plate injecting 2 μL of each sample for analysis. Tandem LC−MS analysis was performed on a Waters Acquity UPLC system interfaced to an AB Sciex QTRAP-5500 or API6500 mass spectrometer utilizing the turbo ion spray interface (AB Sciex, Framingham, MA). Separation was achieved on a Waters Acquity HSS T3 C18 UPLC column (50 × 2.1 mm, 1.8 μm) using a mobile phase consisting of water containing 0.1% formic acid (solvent A) and acetonitrile containing 0.1% formic acid (solvent B) at a flow rate of 0.75 mL/min. Quantification was accomplished by monitoring the MS/MS transition of each peptide. The concentration was determined across a linear concentration range of compound matching standards (standard curve) in the appropriate matrix.

PK parameters were calculated using noncompartmental methods in Watson v.7.4. The area under the plasma concentration−time curve (AUC_{0-t}) was calculated from the first time point up to the last time point using the linear trapezoidal method for ascending concentrations and the log trapezoidal method for descending concentrations. The concentration at 0 h after IV administration was back-extrapolated using the first three time points (0.03, 0.13, and 0.25 h). The remaining area under the plasma concentration−time curve (AUC $t-\infty$) was estimated by dividing the observed concentration at the last time point by the elimination rate constant. This value was added to AUC_{0-t} to estimate the $AUC_{0-\infty}$. The IV plasma clearance was calculated by dividing the dose by $AUC_{0-\infty}$. The terminal half-life of elimination was determined by unweighted linear regression analysis of the log-transformed data. The volume of distribution at steady state (V_{dss}) was obtained from the product of plasma clearance and mean residence time (determined by dividing the extrapolated area under the first moment curve by extrapolated the area under the curve). The maximum plasma concentration (C_{max}) and the time at which maximum concentration occurred (T_{max}) were obtained by graphical inspection of the plasma concentration−time data. For all n = 3, the error is characterized as standard deviation. For n = 2, the error is characterized as the difference between the mean and the individual determinations.

■ ASSOCIATED CONTENT

Supporting Information

The Supporting Information is available free of charge at https://pubs.acs.org/doi/10.1021/acs.jmedchem.0c01084.

Representative LC traces for key molecules in the paper, sample IC_{50} curves for LDLR-FRET and Alexa-FRET assay control peptide, and raw concentration versus time profiles for molecules tested in Mouse IV PK 3D PDB files for each of the new crystal structures have also been uploaded; PDB codes for the crystal structures shown in the paper are as follows: compound **30**, 6XIB; compound **40**, 6XIC; compound **51**, 6XID; compound **78**, 6XIE; and compound **84**, 6XIF; and authors will release the atomic coordinates and experimental data upon article publication (PDF)

6xib (PDB)

6xic (PDB)

6xid (PDB)

6xie (PDB)

6xif (PDB)

■ AUTHOR INFORMATION

Corresponding Author

Thomas J. Tucker − *Departments of Medicinal Chemistry, Merck & Company, Inc., West Point, Pennsylvania 19486, United States;* orcid.org/0000-0001-5616-0802; Email: tom_tucker@merck.com

Authors

Candice Alleyne − *Discovery Pharmaceutical Sciences, Merck & Company, Inc., Kenilworth, New Jersey 07033, United States*

Rupesh P. Amin − *Safety Assessment, Merck & Comapny, Inc., West Point, Pennsylvania 19486, United States*

Bhavana Bhatt − *Safety Assessment, Merck & Comapny, Inc., West Point, Pennsylvania 19486, United States*

Elisabetta Bianchi − *IRBM S.p.A., Pomezia, Rome 00071, Italy*

J. Craig Blain − *UCB Ra Pharma, Cambridge, Massachusetts 02140, United States*

Nicolas Boyer − *UCB Ra Pharma, Cambridge, Massachusetts 02140, United States*

Danila Branca − *IRBM S.p.A., Pomezia, Rome 00071, Italy*

Mark W. Embrey − *Departments of Medicinal Chemistry, Merck & Company, Inc., West Point, Pennsylvania 19486, United States*

Sookhee N. Ha − *Modeling and Informatics, Merck & Company, Inc., Kenilworth, New Jersey 07033, United States*

Kelli Jette − *UCB Ra Pharma, Cambridge, Massachusetts 02140, United States*

Douglas G. Johns − *Discovery Biology, Merck & Company, Inc., Kenilworth, New Jersey 07033, United States*

Angela D. Kerekes − *Departments of Medicinal Chemistry, Merck & Company, Inc., Kenilworth, New Jersey 07033, United States*

Kenneth A. Koeplinger − *Pharmacokinetics Pharmacodynamics and Drug Metabolism, Merck & Company, Inc., West Point, Pennsylvania 19486, United States*

Derek LaPlaca − *UCB Ra Pharma, Cambridge, Massachusetts 02140, United States;* orcid.org/0000-0002-8513-2445

https://dx.doi.org/10.1021/acs.jmedchem.0c01084
J. Med. Chem. XXXX, XXX, XXX−XXX

Nianyu Li − *Safety Assessment, Merck & Comapny, Inc., West Point, Pennsylvania 19486, United States*
Beth Murphy − *Discovery Biology, Merck & Company, Inc., Kenilworth, New Jersey 07033, United States*
Peter Orth − *Structural Sciences, Merck & Company, Inc., Kenilworth, New Jersey 07033, United States*
Alonso Ricardo − *UCB Ra Pharma, Cambridge, Massachusetts 02140, United States*
Scott Salowe − *Discovery Biology, Merck & Company, Inc., Kenilworth, New Jersey 07033, United States*
Kathleen Seyb − *UCB Ra Pharma, Cambridge, Massachusetts 02140, United States*
Aurash Shahripour − *Departments of Medicinal Chemistry, Merck & Company, Inc., Kenilworth, New Jersey 07033, United States*
Joseph R. Stringer − *UCB Ra Pharma, Cambridge, Massachusetts 02140, United States*
Yili Sun − *UCB Ra Pharma, Cambridge, Massachusetts 02140, United States*
Rodger Tracy − *Pharmacokinetics Pharmacodynamics and Drug Metabolism, Merck & Company, Inc., West Point, Pennsylvania 19486, United States*
Chengwei Wu − *Departments of Medicinal Chemistry, Merck & Company, Inc., West Point, Pennsylvania 19486, United States*
Yusheng Xiong − *Departments of Medicinal Chemistry, Merck & Company, Inc., Kenilworth, New Jersey 07033, United States*
Hyewon Youm − *Departments of Medicinal Chemistry, Merck & Company, Inc., Kenilworth, New Jersey 07033, United States*
Hratch J. Zokian − *Discovery Biology, Merck & Company, Inc., Kenilworth, New Jersey 07033, United States*

Complete contact information is available at: https://pubs.acs.org/10.1021/acs.jmedchem.0c01084

Notes

The authors declare no competing financial interest.

■ ACKNOWLEDGMENTS

The authors acknowledge Abbas Walji and H. Blair Wood for helpful discussions and editing related to the manuscript and scientific content. The authors are also grateful to Jennifer Johnston for her excellent graphics work in support of the manuscript.

■ ABBREVIATIONS

ACN, acetonitrile; AOP, tris(dimethylamino)(3*H*-1,2,3-triazolo[4,5-*b*]pyridin-3-yloxy)phosphorus hexafluorophosphate; Boc, *t*-butoxycarbonyl; DBX, di-(1,3-bromomethyl)-benzene; DCM, dichloromethane; DIC, *N*,*N*-diisopropylcarbodiimide; DIEA, diisopropylethyl amine; DMF, dimethylformamide; DMSO, dimethyl sulfoxide; DODT, 3,6-dioxa-1,8-octanedithiol; EtOAc, ethyl acetate; 5F-Trp, 5-fluoro-tryptophan; Fmoc-OSu, Fmoc *N*-hydroxysuccinimide ester; HATU, 1-[bis(dimethylamino)methylene]-1*H*-1,2,3-triazolo[4,5-*b*]-pyridinium 3-oxide hexafluorophosphate; IV, intravenous; ivDde, [l-(4,4-dimethyl-2,6-dioxocyclohex-1-ylidene)-ethyl]-protecting group; LC−MS, liquid chromatography−mass spectrometry; LDL-C, LDL-cholesterol; LDLR, LDL receptor; mAb, monoclonal antibody; Met ID, metabolite identification; NMP, *N*-methyl pyrrolidinone; PCSK9, proprotein convertase subtilisin-like/kexin type 9; PK, pharmacokinetics; PPI, protein−protein interaction; RP-HPLC, reverse phase high performance liquid chromatography; SAR, structure−activity relationship; SPPS, solid phase peptide synthesis; *t*-BuOH, *tert*-butanol; TFA, trifluoroacetic acid; TMS-Cl, trimethylchlorosilane

■ REFERENCES

(1) Sediah, N.G.; Awan, Z.; Chretien, M.; Mbikay, M. PCSK9: A Key Modulator of Cardiovascular Health. *Circ. Res.* **2014**, *114*, 1022−1036.
(2) Szarek, M.; White, H. D.; Schwartz, G. G.; Alings, M.; Bhatt, D. L.; Bittner, V. A.; Chiang, C.; Diaz, R.; Edelberg, J. M.; Goodman, S. G.; Hanotin, C.; Harrington, R. A.; Jukema, J. W.; Kimura, T.; Gabor Kiss, R.; Lecorps, G.; Mahaffey, K. W.; Moryusef, A.; Pordy, R.; Roe, M. T.; Tricoci, P.; Xavier, D.; Zeiher, A. M.; Steg, G. Alcirocumab Reduces Total Nonfatal Cardiovascular and Fatal Events. *J. Am. Coll. Cardiol.* **2019**, *73*, 389−396.
(3) Sabatine, M. S.; Giugliano, R. P.; Keech, A. C.; Honarpour, N.; Wiviott, S. D.; Murphy, S. A.; Kuder, J. F.; Wang, H.; Liu, T.; Wasserman, S. M.; Sever, P. S.; Pedersen, T. R. Evolocumab and Clinical Outcomes in Patients with Cardiovascular Disease. *N. Engl. J. Med.* **2017**, *376*, 1713−1722.
(4) Nasir, K. Just Price for PCSK9 Inhibitors: No Less, No More. *J. Am. Heart Assoc.* **2018**, *7*, No. e010884.
(5) Krähenbühl, S.; Pavik-Mezzour, I.; von Eckardstein, A. Unmet Needs in LDL-C Lowering: When Statins Won't Do! *Drugs* **2016**, *76*, 1175−1190.
(6) Akyea, R. K.; Kai, J.; Qureshi, N.; Iyen, B.; Weng, S. F. Sub-optimal Cholesterol Response to Initiation of Statins and Future Risk of Cardiovascular Disease. *Heart* **2019**, *105*, 975−981.
(7) Yamamoto, T.; Lu, C.; Ryan, R. O. A Two-step Binding Model of PCSK9 Interaction with the Low-Density Lipoprotein Receptor. *J. Biol. Chem.* **2011**, *286*, 5464−5470.
(8) Taechalertpaisarn, J.; Zhao, B.; Liang, X.; Burgess, K. Small Molecule Inhibitors of the PCSK9-LDLR Interaction. *J. Am. Chem. Soc.* **2018**, *140*, 3242−3249.
(9) Stucchi, M.; Grazioso, G.; Lammi, C.; Manara, S.; Zanoni, C.; Arnoldi, A.; Lesma, G.; Silvani, A. Disrupting he PCSK9/LDLR Protein-Protein Interaction by an Imidazole-Based Minimalist Peptidomimetic. *Org. Biomol. Chem.* **2016**, *14*, 9736−9740.
(10) Londregan, A. T.; Wei, L.; Xiao, J.; Lintner, N. G.; Petersen, D.; Dullea, R. G.; McClure, K. F.; Bolt, M. W.; Warmus, J. S.; Coffey, S. B.; Limberakis, C.; Genovino, J.; Thuma, B. A.; Hesp, K. D.; Aspnes, G. E.; Reidich, B.; Salatto, C. T.; Chabot, J. R.; Cate, J. H. D.; Liras, S.; Piotrowski, D. W. Small Molecule PCSK9 Inhibitors: Hit to Lead Optimization of Systemic Agents. *J. Med. Chem.* **2018**, *61*, 5704−5718.
(11) Petrilli, W. L.; Adam, G. C.; Erdmann, R. S.; Abeywickrema, P.; Agnani, V.; Ai, X.; Baysarowich, J.; Byrne, N.; Caldwell, J. P.; Chang, W.; DiNunzio, E.; Feng, Z.; Ford, R.; Ha, S.; Huang, Y.; Hubbard, B.; Johnston, J. J.; Kavana, M.; Lisnock, J.-M.; Liang, R.; Lu, J.; Meng, J.; Orth, P.; Palyha, O.; Parthasarathy, G.; Salowe, S. P.; Sharma, S.; Shipman, J.; Soisson, S. M.; Strack, A. M.; Youm, H.; Zhao, K.; Zink, D. L.; Zokian, H.; Addona, G. H.; Akinsanya, K.; Tata, J. R.; Xiong, Y.; Imbriglio, J. E. From Screening to Targeted Degredation: Strategies for the Discovery and Optimization of Small Molecule Ligands for PCSK9. *Cell Chem. Biol.* **2019**, *27*, 32−40.e3.
(12) Zhang, Y.; Eigenbrot, C.; Zhou, L.; Shia, S.; Li, W.; Quan, C.; Tom, J.; Moran, P.; Di Lello, P.; Skelton, N. J.; Kong-Beltran, M.; Peterson, A.; Kirchhofer, D. Identification of a Small Peptide that Inhibits PCSK9 Protein Binding to the Low-Density Lipoprotein Receptor. *J. Biol. Chem.* **2013**, *289*, 942−955.
(13) Zhang, Y.; Ultsch, M.; Skelton, N. J.; Burdick, D. J.; Beresini, M. H.; Li, W.; Kong-Beltran, M.; Peterson, A.; Quinn, J.; Chiu, C.; Wu, Y.; Shia, S.; Moran, P.; Di Lello, P.; Eigenbrot, C.; Kirchhofer, D. Discovery of a Cryptic Peptide-Binding site on PCSK9 and Design of Antagonists. *Nat. Struct. Mol. Biol.* **2017**, *24*, 848−856.

(14) Pelay-Gimeno, M.; Glas, A.; Koch, O.; Grossmann, T. N. Structure-Based Design of Inhibitors of Protein − Protein Interactions: Mimicking Peptide Binding Epitopes. *Angew. Chem., Int. Ed.* **2015**, *54*, 8896−8927.
(15) Dyrbuś, K.; Gąsior, M.; Penson, P.; Ray, K. K.; Banach, M. Inclisiran − New Hope in the Management of Lipid Disorders. *J. Clin. Lipidol.* **2020**, *14*, 16−27.
(16) Xu, S.; Luo, S.; Zhu, Z.; Xu, J. Small Molecules as Inhibitors of PCSK9: Current Status and Future Challenges. *Eur. J. Med. Chem.* **2019**, *162*, 212−233.
(17) Lavecchia, A.; Cerchia, C. Recent Advances in Developing PCSK9 Inhibitors for Lipid-Lowering Therapy. *Future Med. Chem.* **2019**, *11*, 423−441.
(18) Wang, Y.; Liu, Z.-P. PCSK9 Inhibitors: Novel Therapeutic Strategies for Lowering LDL Cholesterol. *Mini-Rev. Med. Chem.* **2019**, *19*, 165−176.
(19) Vinogradov, A. A.; Yin, Y.; Suga, H. Macrocyclic Peptides as Drug Candidates: Recent Progress and Remaining Challenges. *J. Am. Chem. Soc.* **2019**, *141*, 4167−4181.
(20) Josephson, K.; Ricardo, A.; Szostak, J. W. mRNA Display: From Basic Principles to Macrocycle Drug Discovery. *Drug Discovery Today* **2014**, *19*, 388−399.
(21) Huang, Y.; Wiedmann, M. M.; Suga, H. RNA Display Methods for the Discovery of Bioactive Macrocycles. *Chem. Rev.* **2019**, *119*, 10360−10391.
(22) Kerekes, A. D. Unpublished results from our laboratories. A manuscript describing the alternative series of PCSK9 molecules is currently in preparation.
(23) Böhm, H.-J.; Banner, D.; Bendels, S.; Kansy, M.; Kuhn, B.; Müller, K.; Obst-Sander, U.; Stahl, M. Fluorine in Medicinal Chemistry. *ChemBioChem* **2004**, *5*, 637−643.
(24) McNeil, B. D.; Pundir, P.; Meeker, S.; Han, L.; Undem, B. J.; Kulka, M.; Dong, X. Indentification of a Mast-Cell-Specific Receptor Crucial for Pseudo-allergic Drug Reactions. *Nature* **2015**, *519*, 237−241.
(25) Subramanian, H.; Gupta, K.; Ali, H. Roles of Mas-related G Protein-Coupled Receptor X2 on Mast Cell-Mediated Host Defense, Pseudoallergic Drug Reactions, and Inflammatory Diseases. *J. Allergy Clin. Immunol.* **2016**, *138*, 700−710.
(26) Hein, C. D.; Liu, X.-M.; Wang, D. Click Chemistry, A Powerful Tool for Pharmaceutical Sciences. *Pharm. Res.* **2008**, *25*, 2216−2230.
(27) Barral, K.; Moorhouse, A. D.; Moses, J. E. Efficient Conversion of Aromatic Amines into Azides: A One-Pot Synthesis of Triazole Linkages. *Org. Lett.* **2007**, *9*, 1809−1811.
(28) Han, S.-Y.; Kim, Y.-A. Recent Development of Peptide Coupling Reagents in Organic Synthesis. *Tetrahedron* **2004**, *60*, 2447−2467.
(29) Bricogne, G.; Blanc, E.; Brandl, M.; Flensburg, C.; Keller, P.; Paciorek, W.; Roversi, P.; Sharff, A.; Smart, O.; Vonrhein, C.; Womack, T. (2017) *BUSTER*, version 2.11.6. Cambridge, United Kingdom: Global Phasing Ltd.
(30) Winn, M. D.; Ballard, C. C.; Cowtan, K. D.; Dodson, E. J.; Emsley, P.; Evans, P. R.; Keegan, R. M.; Krissinel, E. B.; Leslie, A. G. W.; McCoy, A.; McNicholas, S. J.; Murshudov, G. N.; Pannu, N. S.; Potterton, E. A.; Powell, H. R.; Read, R. J.; Vagin, A.; Wilson, K. S. Overview of the CCP4 Suite and Current Developments. *Acta Crystallogr., Sect. D: Biol. Crystallogr.* **2011**, *67*, 235−242.
(31) Emsley, P.; Lohkamp, B.; Scott, W. G.; Cowtan, K. Features and Development of Coot. *Acta Crystallogr., Sect. D: Biol. Crystallogr.* **2010**, *66*, 487−501.
(32) Wlodek, S.; Skillman, A. G.; Nicholls, A. Automated Ligand Placement and Refinement with a Combined Force Field and Shape Potential. *Acta Crystallogr., Sect. D: Biol. Crystallogr.* **2006**, *62*, 741−749.
(33) Rothschild, A. M. Mechanisms of Histamine Release by Compound 48/80. *Br. J. Pharmacol.* **1970**, *38*, 253−262.

https://dx.doi.org/10.1021/acs.jmedchem.0c01084
J. Med. Chem. XXXX, XXX, XXX−XXX